

# Quantum entanglement in the one-dimensional spin-orbital $SU(2) \otimes XXZ$ model

Wen-Long You,<sup>1,2</sup> Peter Horsch,<sup>1</sup> and Andrzej M. Oleś<sup>1,3</sup>

<sup>1</sup>*Max-Planck-Institut für Festkörperforschung, Heisenbergstrasse 1, D-70569 Stuttgart, Germany*

<sup>2</sup>*College of Physics, Optoelectronics and Energy, Soochow University, Suzhou, Jiangsu 215006, People's Republic of China*

<sup>3</sup>*Marian Smoluchowski Institute of Physics, Jagiellonian University, prof. S. Łojasiewicza 11, PL-30348 Kraków, Poland*

(Dated: October 4, 2021)

We investigate the phase diagram and the spin-orbital entanglement of a one-dimensional  $SU(2) \otimes XXZ$  model with  $SU(2)$  spin exchange and anisotropic  $XXZ$  orbital exchange interactions and negative exchange coupling. As a unique feature, the spin-orbital entanglement entropy in the entangled ground states increases here linearly with system size. In the case of Ising orbital interactions we identify an emergent phase with long-range spin-singlet dimer correlations triggered by a quadrupling of correlations in the orbital sector. The peculiar translational invariant spin-singlet dimer phase has finite von Neumann entanglement entropy and survives when orbital quantum fluctuations are included. It even persists in the isotropic  $SU(2) \otimes SU(2)$  limit. Surprisingly, for finite transverse orbital coupling the long-range spin singlet correlations also coexist in the antiferromagnetic spin and alternating orbital phase making this phase also unconventional. Moreover we also find a complementary orbital singlet phase that exists in the isotropic case but does not extend to the Ising limit. The nature of entanglement appears essentially different from that found in the frequently discussed model with positive coupling. Furthermore we investigate the collective spin and orbital wave excitations of the disentangled ferromagnetic-spin/ferro-orbital ground state and explore the continuum of spin-orbital excitations. Interestingly one finds among the latter excitations two modes of exciton bound states. Their spin-orbital correlations differ from the remaining continuum states and exhibit logarithmic scaling of the von Neumann entropy with increasing system size. We demonstrate that spin-orbital excitons can be experimentally explored using resonant inelastic x-ray scattering, where the strongly entangled exciton states can be easily distinguished from the spin-orbital continuum.

PACS numbers: 75.25.Dk, 03.67.Mn, 05.30.Rt, 75.10.Jm

## I. INTRODUCTION

Spin-orbital coupling phenomena are ubiquitous in solids and have been known to exist since the early days of quantum mechanics and band theory, but only recently it was realized that the quantum nature of orbital degrees of freedom plays a crucial role in the fields of strongly correlated electrons [1–7] and cold atoms [8–12]. The growing evidence of spin-orbital entanglement (SOE) accumulated due to novel experimental techniques which probe a variety of underlying electronic states. The strong Coulomb interactions and the relativistic spin-orbit interaction entangle locally the spin and orbital degrees of freedom [13] which display an amazing variety of fundamentally new and fascinating phenomena, ranging from topologically nontrivial states [14], relativistic Mott-insulating behavior in  $5d$  [15, 16] and  $4d$  [17, 18] transition-metal oxides and entanglement on superexchange bonds in spin-orbital models [6, 19]. Other more recent developments include entangled spin-orbital excitations [20, 21], doped spin-orbital systems [22], skyrmion lattices in the chiral metal MnSi [23], multiferroics, spin-Hall effects [24], Majorana and Weyl fermions [25], topological surface states [26], Kondo systems [27], exotic spin textures in disordered systems, to name just a few.

To date, experimental observation of a dynamic spin-orbital state has been a challenge. Apart from the in-

trinsic anisotropy and the relative complexity of the orbital couplings, it has been shown that the interplay between the two frustrated degrees of freedom may lead to exotic states of matter. An x-ray scattering study of a dynamic spin-orbital state in the frustrated magnet  $Ba_3CuSb_2O_9$  supports spin liquid state [28, 29], while  $FeSc_2S_4$  [30–32] and the  $d^1$  effective models on the triangular lattice [33] and on the honeycomb lattice [34, 35] are found to be candidates for spin-orbital liquids in the theory. Recently remarkable progress was achieved due to rapidly developed resonant inelastic x-ray scattering (RIXS) techniques [36] which helped to explore the elementary excitations in  $Sr_2CuO_3$  [37, 38] and  $Sr_2IrO_4$  [39], with antiferromagnetic (AF) and ferro-orbital (FO) order in ground states. Orbital order in the spin-gapped dimerised system  $Sr_3Cr_2O_8$  below the Jahn-Teller transition was also identified [40]. However, it remains challenging experimentally and theoretically, mainly owing to the lack of an ultimate understanding of spin-orbital correlations.

In the Mott insulators with an idealized perovskite structure, the low-energy physics is described by spin-orbital models, similar to the Kugel-Khomskii model [2], where the spin and orbital are considered on equal footing as dynamic quantum variables [4]. Spin interaction possesses  $SU(2)$  symmetry, which will be broken however by the relativistic spin-orbit coupling. It couples spins

to the orbitals, that are in general non-SU(2)-symmetric in a solid. However, this coupling can frequently be neglected in realistic 3d systems and one is left in general with entangled spin-orbital superexchange problem [6], that is the eigenstates cannot be written as products of spin and orbital wave functions. One immediate consequence of entanglement is that spin and orbital terms cannot be factorized in the mean-field approach. Orbitals are spatially anisotropic and thus their interactions have lower symmetry than the spin ones which reflects the directional dependence of the orbital wave functions. For the fixed occupation of orbitals, the magnitude and sign of the spin-orbital superexchange interactions follow the classical Goodenough-Kanamori rules [41], but quantum fluctuations change them and make it necessary to consider spin-orbital interplay in entangled states on exchange bonds [19]. Therefore, it is important to measure whether eigenstates are entangled or not.

A natural measure of SOE is the von Neumann entropy (vNE) which we write first for the nondegenerate ground state  $|\Psi_0\rangle$ ,

$$\mathcal{S}_{\text{vN}}^0 \equiv -\text{Tr}_A\{\rho_A^{(0)} \log_2 \rho_A^{(0)}\}. \quad (1.1)$$

Here we consider a system  $\Omega$  composed of two non-overlapping subsystems [42], i.e.,  $\Omega = A \cup B$ ,  $A \cap B = \emptyset$ , and  $\rho_A^{(0)}$  is the reduced density matrix. It is obtained by integrating the density matrix over subsystem  $B$ , i.e.,  $\rho_A^{(0)} = \text{Tr}_B|\Psi_0\rangle\langle\Psi_0|$ . However, one has to realize that information contained in entanglement entropy depends crucially on how one partitions the Hilbert space of the system. To investigate SOE we use here as two subsystems  $A$  and  $B$  the spin and orbital degrees of freedom in the entire chain. Standard spin-orbital phases may have entanglement in only one sector and here we concentrate on joint SOE [43]. This choice is distinct from the one conventionally made when the system is separated into two spatially complementary parts [44], for instance in frustrated spin chains [45] or in the periodic 1D Anderson model [46].

Though much attention was devoted to the ground state in the past [47], it has been noticed only recently that the entanglement entropy of low-energy excitations may provide even more valuable insights [43, 48, 49] which are of crucial importance to understand the origin of quantum phase transitions in spin-orbital systems [50]. The well known area law of the bipartite entanglement entropy restricts the Hilbert space accessible to a ground state of gapped systems [51, 52], while the area law is violated by a leading logarithmic correction in critical systems, whose prefactor is determined by the number of chiral modes and precisely given by Widom conjecture [53]. In this respect, the application of the entanglement entropy in describing quantum criticality in many-body Hamiltonian merits a lot of studies [42, 54].

On the other hand, the excited states have the mixture of logarithmic and extensive entanglement entropy, and the logarithmic states are expected to be negligible

in number compared to all the others. The entanglement in excited state is proven always larger than that of the ground state of a spin chain [55]. For a spin-orbital coupled system, the division of spin and orbital operators retains the real-space symmetries, which is beneficial to the calculation of mutual entanglement. In two-particle states, the SOE is determined by the inter-component coherence length [43], as though the state has sufficient decay of correlations [45].

The aim of this paper is to use the entanglement entropy to investigate the full phase diagram of the one-dimensional (1D) anisotropic spin-orbital SU(2) $\otimes$ XXZ model. The main motivation for considering the Ising asymmetry in the orbital sector comes from the observation that spin-orbital entanglement is large when both subsystems, i.e., spin and orbital sectors, reveal strong quantum fluctuations. Thus the Ising anisotropy which is present in many physical systems introduces additional control of orbital fluctuations and thereby provides an important control parameter for SOE. Here we focus on the model with negative exchange interaction. This choice of the exchange coupling restricts somewhat joint spin-orbital fluctuations being particularly large near the SU(4) symmetric point in the 1D spin-orbital model with *positive* coupling constant [56], but opens novel possibilities for entangled states, as we show below [50]. An interesting phase with entangled ground state, consisting of alternating spin singlets along the spin-orbital ring, is found for Ising orbital interactions when the dimerization in the spin channel induces the change from FO to alternating orbital (AO) correlations. Here we report the complete phase diagram of the anisotropic SU(2) $\otimes$ XXZ spin-orbital model, with two phases of similar nature which gain energy from singlet correlations leading to dimerization, either in spin or in orbital sector. These phases were overlooked before in the fully symmetric case, i.e., in the phase diagram of the isotropic SU(2) $\otimes$ SU(2) model [43].

We also analyze the nature of spin-orbital excited states, particularly in the case of the disentangled ferromagnetic (FM) and FO ground state, labeled as FM/FO order. We also analyze entanglement entropy in the excited states for the FM/FO phase and show that spin-orbital excitations form a continuum, supplemented by collective bound states. The latter states are characterized by a logarithmic scaling behavior, and as we show could be detected by properly designed RIXS experiments [57–59].

The paper is organized as follows. The model is introduced in Sec. II. In Sec. III we present an analytic solution for the ground state in the Ising limit of the orbital interactions. A more general situation with anisotropic XXZ orbital interaction is analyzed in Sec. IV A, and the phase diagram for the isotropic SU(2) $\otimes$ SU(2) model is reported in Sec. IV B. This model and the obtained SOE are different from the AF case, as shown in Sec. IV C. Next we determine the elementary excitations in the FM/FO phase in Sec. V and show that they are en-

tangled although the ground state is disentangled. The vNE spectral function is presented in Sec. VIA, including the scaling behavior of the bound states which is contrasted with that in the AF/AO ground state. In Sec. VIB we explore the possibilities of investigating entanglement in the present 1D spin-orbital model by RIXS. The paper is concluded by a discussion and brief summary in Sec. VII. Some additional technical insights which are accessible by an exact solution of the two-site model are presented in the Appendix.

## II. THE 1D SPIN-ORBITAL $SU(2) \otimes XXZ$

We consider the 1D spin-orbital Hamiltonian which couples  $S = 1/2$  spins and  $T = 1/2$  orbital (pseudospin) operators,

$$\mathcal{H} = -J \sum_j \mathcal{H}_j^S(x) \otimes \mathcal{H}_j^T(\Delta, y), \quad (2.1)$$

with  $SU(2)$  spin Heisenberg interaction  $\mathcal{H}_j^S(x)$ , orbital anisotropic  $XXZ$  interaction  $\mathcal{H}_j^T(\Delta, y)$ ,

$$\mathcal{H}_j^S(x) = \vec{S}_j \cdot \vec{S}_{j+1} + x, \quad (2.2)$$

$$\mathcal{H}_j^T(\Delta, y) = \Delta (T_j^x T_{j+1}^x + T_j^y T_{j+1}^y) + T_j^z T_{j+1}^z + y. \quad (2.3)$$

We take below  $J = 1$  as the energy unit. The model Eq. (2.1) has the following parameters: (i)  $x$  and  $y$  which determine the amplitudes of orbital and spin ferro-exchange interactions,  $-Jx$  and  $-Jy$ , respectively, and (ii)  $\Delta$  which interpolates between the Heisenberg ( $\Delta = 1$ ) and Ising ( $\Delta = 0$ ) limit for orbital interactions. When  $\Delta = 1$ , the spin and orbital interactions are on equal footing and the symmetry of the Hamiltonian (2.1) is enhanced to  $SU(2) \otimes SU(2)$  — this model describes a generic competition between FM and AF spin, and between FO and AO bond correlations [43].

We emphasize that the coupling constant  $-J$  is *negative*, so at large  $x > 0$  and  $y > 0$  it gives a disentangled FM/FO ground state, see below — therefore the model may be called in short FM. This choice of the exchange coupling restricts somewhat joint spin-orbital fluctuations being large near the  $SU(4)$  symmetric point,  $(x, y) = (0.25, 0.25)$ , in the 1D spin-orbital model with *positive*, i.e., AF coupling constant [56], but opens other interesting possibilities for entangled states, as we have shown recently [50]. Both total spin magnetization  $S^z$  and orbital polarization  $T^z$  are conserved, and time reversal symmetry leads to the total momentum either  $k = 0$  or  $k = \pi$ .

Before analyzing the spin-orbital model of Eq. (1) in more detail, let us summarize briefly the properties of the well known AF model, with positive coupling constant  $J$ . The  $SU(4)$  symmetric Hamiltonian found at  $(x, y) = (0.25, 0.25)$  is an integrable model which can be solved in terms of the Bethe *Ansatz* [56, 60]. Away from the  $SU(4)$  symmetric points this choice of the coupling constant favors the phases with spin-orbital order

depending on the actual values of  $x$  and  $y$ , and the phase diagram obtained by numerical methods includes in general phases with all types of coupled spin-orbital order, i.e., FM/FO, AF/FO, AF/AO, and FM/AO, as well as the gapless spin-orbital liquid phase near the  $SU(4)$  point [61, 62]. In addition, Schwinger boson analysis gives phases with spin-orbital valence-bond correlations and also spin valence bond and orbital valence-bond phases [63]. The latter two show a tendency towards dimerised spin or orbital correlations which occur here in the proximity of the  $SU(4)$  point. For some special choice of parameters the model can be solved exactly: (i) when  $\Delta = 1$  and  $x = y = 3/4$ , the exact ground state is doubly degenerate with the spins and the orbitals forming singlets on alternate bonds, while (ii) when  $\Delta = 0$ ,  $x = 3/4$  and  $y = 1/2$ , the non-Haldane spin-liquid ground state can be analytically obtained [64, 65], and (iii) several integrable cases were presented for interactions with special symmetries [66, 67], or (iv) with  $XY$  orbital interactions ( $\Delta = \infty$ ) [20].

The form of Eq. (2.1) is not the most general one but is representative for real spin-orbital systems with anisotropic orbital interactions. In real systems the orbital part contributes by additional superexchange terms which are not coupled to  $SU(2)$  spin interaction [4]. For instance, in the case of  $t_{2g}$  orbital degrees of freedom as in the perovskite titanates or vanadates, the interactions along the  $c$  cubic axis involve the doublet of two orbitals active along it, i.e., the  $yz$  and  $zx$  orbitals [68]; a similar situation is encountered in a tetragonal crystal field of a quasi-1D Mott insulator [69], or for  $p_x$  and  $p_y$  orbitals of a 1D fermionic optical lattice [8–10].

*A priori*, due to the quartic spin-orbital joint term,  $\propto (\vec{S}_j \cdot \vec{S}_{j+1})[\Delta(T_j^x T_{j+1}^x + T_j^y T_{j+1}^y) + T_j^z T_{j+1}^z]$  in the Hamiltonian Eq. (2.1) the spin-orbital interactions are entangled, and the spin and orbital operators cannot be separated from each other in the correlation function, except for some ground or excited states in which the SOE vanishes. The spin-orbital bond correlations (2.4)

$$C_1^{\text{tot}} \equiv \left\langle (\vec{S}_j \cdot \vec{S}_{j+1})[\Delta(T_j^x T_{j+1}^x + T_j^y T_{j+1}^y) + T_j^z T_{j+1}^z] \right\rangle, \quad (2.4)$$

are uniform in the considered system and  $C_1^{\text{tot}}$  does not depend on the site index  $j$ . We investigate below these composite quartic correlations and show that they could also be surprisingly large. As an additional criterion of setting up the phase diagram, we use below the fidelity susceptibility which elucidates the change rate of ground states in the parameter space [70]. It serves as an order parameter to characterize the phase diagram of the anisotropic ( $\Delta < 1$ ) spin-orbital model (2.1). The fidelity susceptibility is defined as follows,

$$\chi_F(\lambda) \equiv -2 \lim_{\delta\lambda \rightarrow 0} \frac{\ln \mathcal{F}(\lambda, \delta\lambda)}{(\delta\lambda)^2}, \quad (2.5)$$

where the fidelity

$$\mathcal{F}(\lambda, \delta\lambda) = |\langle \Psi_0(\lambda) | \Psi_0(\lambda + \delta\lambda) \rangle|, \quad (2.6)$$

is taken along a certain path in the parameter space in the vicinity of the point  $\lambda \equiv \lambda(\Delta, x, y)$ .

### III. ISING ORBITAL INTERACTIONS ( $\Delta = 0$ )

In the Ising limit of orbital interactions ( $\Delta = 0$ ) the Hamiltonian (2.1) simplifies and has  $SU(2) \otimes \mathbb{Z}_2$  symmetry — it is a prototype model for the directional orbital interactions with quenched quantum fluctuations in  $t_{2g}$  systems. This may happen in real compounds in two ways: (i) either only one of the two active orbitals is occupied by one electron and contributes in the hopping processes along the  $180^\circ$  bonds [71] or  $90^\circ$  bonds [72], or (ii) the orbital degrees of freedom are quenched in the presence of strong crystal field. In both these cases the orbital exchange (orbital-flip) processes are blocked and orbital interaction are of a classical Ising-like form. Such Ising interactions are frustrated when they emerge in higher dimension, as in the well-studied orbital compass model [73–75] and in Kitaev model [76], see also a recent review on the compass model [77]. It is now intriguing to ask what happens to the SOE in this case. It may be still triggered by spin fluctuations while the model with Ising spin interactions (A.2) is classical.

The phase diagram of the model Eq. (2.1) at  $\Delta = 0$ , i.e., in the absence of orbital fluctuations, which follows from fidelity susceptibility (2.5) is displayed in Fig. 1. As expected, one finds four trivial combinations of spin-orbital order: FM/FO (phase I), AF/FO (phase II), AF/AO (phase III), and FM/AO (phase IV). All these phases have the entanglement entropy (1.1)  $\mathcal{S}_{\text{vN}}^0 = 0$  and spins and orbitals disentangle. Transitions between pairs of them are given by straight lines and may be also obtained rigorously by the mean-field approach. The ground state of a  $L$ -site chain stays in the subspace  $S^z = 0$ ,  $T^z = 0$ , momentum  $k = 0$  (always degenerate with  $S^z = 0$ ,  $T^z = 0$ ,  $k = \pi$  for all parameters) in phases III (AF/AO), IV (FM/AO) and V, while it is found in the subspaces  $S^z = 0$ ,  $T^z = \pm L/2$ ,  $k = 0$  in phases I (FM/FO) and II (AF/FO) (of course, in phases I and IV also other values of  $S^z \neq 0$ , with  $-L/2 \geq S^z \geq L/2$ , are allowed and the ground states have the respective degeneracy). The ground states with energy  $E_0 = 0$  are highly degenerate when  $x < -1/4$  along the critical line  $y = 1/4$  between phases III and IV, suggesting that antiparallel orbitals erase the spin dynamics. Along the critical line  $y = -1/4$  between phases I and II, the ground states are also highly degenerate when  $x \geq 3/4$ , and parallel orbitals on the bonds (in FO order) quench again the spin fluctuations.

Although the orbital interactions are Ising-like, entangled spin-orbital ground state occurs in phase V. In order to understand better emergent phase V, we introduce the longitudinal equal-time spin/orbital structure factor, defined for a ring of length  $L$  (with a lattice constant  $a = 1$ ;

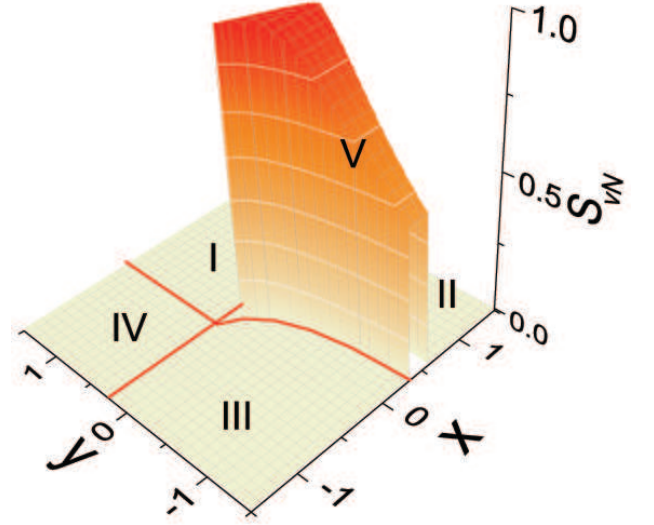


FIG. 1. (Color online) Spin-orbital entanglement entropy  $\mathcal{S}_{\text{vN}}^0$  Eq. (1.1) and the phase diagram in the  $(x, y)$  plane of the  $SU(2) \otimes \mathbb{Z}_2$  spin-orbital model (2.1) with  $\Delta = 0$  as obtained for the system size of  $L = 8$  sites. The critical lines are discerned by both fidelity susceptibility and analytical method. Phases I-IV are disentangled ( $\mathcal{S}_{\text{vN}}^0 = 0$ ) with order defined as follows: FM/FO (phase I), AF/FO (phase II), AF/AO (phase III), and FM/AO (phase IV). The spin and orbital textures in phase V with finite entropy  $\mathcal{S}_{\text{vN}}^0 > 0$  are explained in the text.

we use periodic boundary conditions) by

$$S^{zz}(k) = \frac{1}{L} \sum_{j,j'=1}^L e^{-ik(j-j')} \langle S_j^z S_{j'}^z \rangle, \quad (3.1)$$

$$T^{zz}(k) = \frac{1}{L} \sum_{j,j'=1}^L e^{-ik(j-j')} \langle T_j^z T_{j'}^z \rangle. \quad (3.2)$$

The calculation of the equal-time structure factor  $S^{zz}(k)$  for a model of uncorrelated nearest neighbor dimers was compared with the one for the kagome lattice  $\text{ZnCu}_3(\text{OD})_6\text{Cl}_2$  [78]. One finds analytically that in the case  $\Delta = 0$ , a cosine-like spin structure factor, i.e.,  $S^{zz}(k) \propto (1 - \cos k)$ , is revealed in phase V for  $y = -1/4$ , implying that only nearest neighbor spins are correlated. This finding is essential as the short-range spin correlation indicates here a translation invariant dimerised spin-singlet state which has the same spin structure as the Majumdar-Ghosh (MG) spin state [79]. However, this state is not triggered here by frustrated interactions  $J_1$  and  $J_2$ , but is evidently induced by the correlations in the orbital sector.

In the Ising limit we obtain the analytic ground state for phase V as described below. The essential feature is that the energy is gained by spin singlets occupying the bonds with AO states, while the bonds connecting two spin singlets have FO order, see Fig. 2(a). To construct the ground state, we introduce the corresponding four



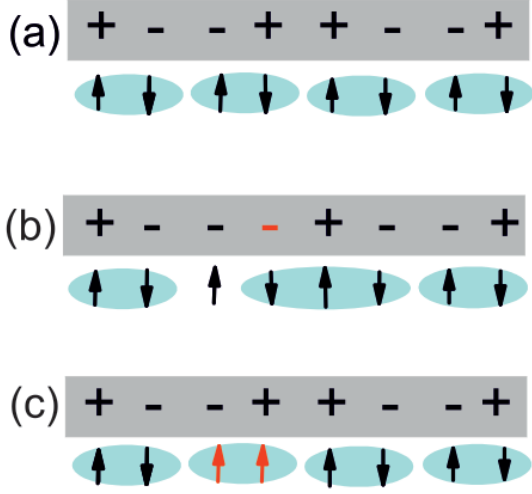


FIG. 2. (Color online) (a) One of four translational equivalent spin and orbital configurations in the Ising limit of the spin-orbital model (2.1) at  $\Delta = 0$  and  $y = -0.25$ . The spins form isolated dimers (shaded ovals). (b) A single orbital excitation and induced spin configuration. (c) A single spin flip makes a singlet-triplet spin excitation, but does not induce any change in orbital correlations.

configurations in the orbital sector:

$$\begin{aligned} |\phi_1\rangle &= |++--++--\dots\rangle, \\ |\phi_2\rangle &= | - + + - - + + - \dots\rangle, \\ |\phi_3\rangle &= | -- ++ -- ++ \dots\rangle, \\ |\phi_4\rangle &= | + - - + + - - + \dots\rangle. \end{aligned} \quad (3.3)$$

The solutions are classified by the momenta corresponding to the translational symmetry of the system. The orbital wave functions in the ground state for the momenta  $k = 0, \pi/2, 3\pi/2, \pi$  correspond to:

$$|\phi_k\rangle = \frac{1}{2} (|\phi_1\rangle + e^{ik}|\phi_2\rangle + e^{2ik}|\phi_3\rangle + e^{3ik}|\phi_4\rangle). \quad (3.4)$$

In spin subspace there are two distinct (but nonorthogonal) states:

$$\begin{aligned} |\psi_1^D\rangle &= [1, 2][3, 4] \dots [N-1, N], \\ |\psi_2^D\rangle &= [2, 3][4, 5] \dots [N, 1], \end{aligned} \quad (3.5)$$

where the singlets are located on odd (even) bonds. Here a singlet is defined by  $[l, l+1] = (|\uparrow\downarrow\rangle - |\downarrow\uparrow\rangle)/\sqrt{2}$ .

One representative component of the ground state with the orbital part  $|\phi_4\rangle$  accompanied by the spin state  $|\psi_1^D\rangle$  is shown in Fig. 2(a). The ground state in the  $k = 0$  subspace is given by the superposition

$$\begin{aligned} |\Phi_{k=0}\rangle &= \\ &= \frac{1}{2} (|\phi_1\rangle \otimes |\psi_2^D\rangle + |\phi_2\rangle \otimes |\psi_1^D\rangle + |\phi_3\rangle \otimes |\psi_2^D\rangle + |\phi_4\rangle \otimes |\psi_1^D\rangle) \\ &= \frac{1}{\sqrt{2}} \left( \frac{|\phi_1\rangle + |\phi_3\rangle}{\sqrt{2}} \otimes |\psi_2^D\rangle + \frac{|\phi_2\rangle + |\phi_4\rangle}{\sqrt{2}} \otimes |\psi_1^D\rangle \right). \end{aligned} \quad (3.6)$$

The state  $|\Phi_{k=0}\rangle$  is entangled both in individual spin and orbital subspaces, and also is characterized by SOE along the chain. Such a many-body state, and similar states obtained for other momenta,  $k = \pm\pi/2$  and  $k = \pi$ , give an exact value of the vNE,  $S_{\text{vN}}^0 = 1$ . The resulting fluctuations between these states suppress conventional order and the system features finite entropy even at zero temperature, in contrast to the naive expectation from the third law of thermodynamics. The emergent excitations are also entangled and fundamentally different from the individual spin or orbital ones, see Figs. 2(b) and 2(c).

As the orbital correlations are classical in the Ising limit, we can determine all the phase boundaries analytically by considering the spin interactions for various orbital configurations. The lower boundary between phase III (AF/AO) and V at  $y = -1/4$  can be determined by comparing the uniform state with energies of AO correlation on a bond, i.e.,  $\langle T_j^z T_{j+1}^z \rangle = -1/4$ , with the alternating state of pairs of the same orbitals shown in Fig. 2(a), i.e.,  $\langle T_j^z T_{j+1}^z \rangle = (-1)^j/4$ , which coexists with spin dimer order (spin interactions vanish for a pair of identical orbitals). One finds the following effective spin Hamiltonian in this case:

$$H_{\text{DIM}} = \frac{1}{2} \sum_{j \in \text{odd}} (\vec{S}_j \cdot \vec{S}_{j+1} + x), \quad (3.7)$$

and the corresponding ground state energy per site in the thermodynamic limit is

$$E_{\text{DIM}}^0 = \frac{1}{4} (-0.75 + x). \quad (3.8)$$

The dimerised phase competes with the AO order coexisting with the 1D resonating valence-bond spin state, with energy

$$E_{\text{AO}}^0 = \frac{1}{2} (-0.4431 + x). \quad (3.9)$$

Hence, one finds that  $E_{\text{DIM}}^0 < E_{\text{AO}}^0$  for  $x > 0.136$ . The quadrupling due to spin-orbital interplay in phase V is well seen by the calculation of the four-spin correlation function which we define following Refs. [80, 81],

$$\begin{aligned} D(r) &= \frac{1}{L} \sum_i \left[ \langle (\vec{S}_i \cdot \vec{S}_{i+1})(\vec{S}_{i+r} \cdot \vec{S}_{i+r+1}) \rangle \right. \\ &\quad \left. - \langle \vec{S}_i \cdot \vec{S}_{i+1} \rangle \langle \vec{S}_{i+r} \cdot \vec{S}_{i+r+1} \rangle \right]. \end{aligned} \quad (3.10)$$

If  $y = -1/4$ , spin dimer correlations alternate and

$$D(r) = (-1)^r \left( \frac{3}{8} \right)^2, \quad (3.11)$$

which follows from Eq. (3.10) for the alternating spin singlets,  $\langle \vec{S}_i \cdot \vec{S}_{i+r} \rangle = -3[1 - (-1)^r]/8$ . Indeed, one finds this value (3.11) for  $x \in [0.2, 0.7]$  and the result is robust and the same for systems sizes  $L = 12$  and  $L = 16$ , see Fig. 3. On the contrary, for  $x < 0.2$  the values of  $D(r)$

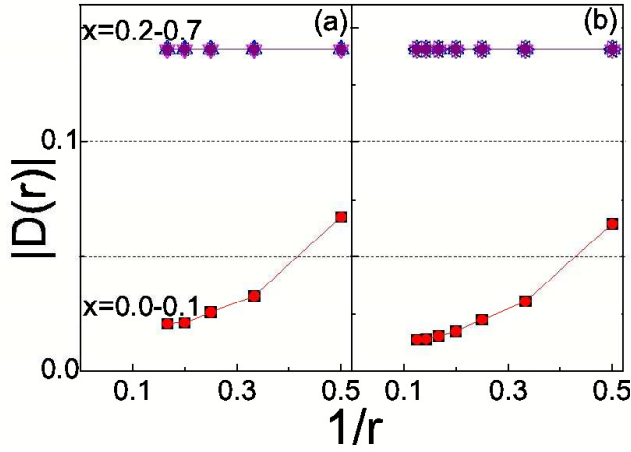


FIG. 3. Dimer correlation function  $D(r)$  (3.10) obtained for the anisotropic  $SU(2) \otimes \mathbb{Z}_2$  spin-orbital model for different values of  $x \in [0, 0.7]$  in phases V and III and for the ring of length: (a)  $L = 12$ , and (b)  $L = 16$  sites. Parameters:  $y = -0.25$  and  $\Delta = 0$ .

decrease with increasing distance  $r$ , and would vanish in the thermodynamic limit of  $L \rightarrow \infty$ .

When  $y < -1/4$ , there are three competing phases with predetermined orbital configurations (AO, DIM, or FO) and the corresponding spin interactions given by effective spin Hamiltonians:

$$H_{AO} = \left(\frac{1}{4} - y\right) \sum_j (\vec{S}_j \cdot \vec{S}_{j+1} + x), \quad (3.12)$$

$$H_{DIM} = \left(\frac{1}{4} - y\right) \sum_{j \in \text{odd}} (\vec{S}_j \cdot \vec{S}_{j+1} + x) - \left(\frac{1}{4} + y\right) \sum_{j \in \text{even}} (\vec{S}_j \cdot \vec{S}_{j+1} + x), \quad (3.13)$$

$$H_{FO} = -\left(\frac{1}{4} + y\right) \sum_j (\vec{S}_j \cdot \vec{S}_{j+1} + x). \quad (3.14)$$

In this case also even inter-singlet bonds contribute to the energy in the  $|DIM\rangle$  state, but the spin correlations vanish, i.e.,  $\langle \vec{S}_j \cdot \vec{S}_{j+1} \rangle = 0$ . It is obvious that  $H_{AO}$  and  $H_{FO}$  stand for the same (translational invariant) spin Hamiltonian, and  $H_{FO}$  will have lower ground state energy when  $x > -\langle \vec{S}_j \cdot \vec{S}_{j+1} \rangle_{AF} \simeq 0.4431$ . The dimerised AF Heisenberg chain (3.13) related to spin-Peierls state cannot be solved trivially, with the exception of the free-dimer limit ( $y = -0.25$ ) and the uniform Heisenberg limit ( $y = -\infty$ ) [82]. One finds the ground state energy per site  $\varepsilon_\infty(\delta)$  of a pure dimerised spin chain [83],

$$\varepsilon_\infty(\delta) = \frac{3}{4} \frac{1}{1 + \alpha} \left( 1 + \frac{\alpha^2}{8} + \frac{\alpha^3}{32} + \dots \right), \quad (3.15)$$

with  $\alpha = (1 - \delta)/(1 + \delta)$  and  $\delta \equiv 1/|4y| \gtrsim 0.4$ . For  $\delta \lesssim 0.4$ ,

$$\varepsilon_\infty(\delta) = \ln 2 - (\ln 2 - 1)|\delta|^{4/3}. \quad (3.16)$$

In such a case,  $E_{DIM}^0 = y[\varepsilon_\infty(\delta) - x]$ . The overwhelming dimerised phase will persist in a range of negative values of  $y$ , and the boundaries close at  $y = -\infty$ , as is indicated by structure factors and fidelity susceptibility.

The phase transitions in the phase diagram of Fig. 1 imply the discontinuous changes of order parameters in first-order quantum phase transitions. The orbital order changes from phase II (AF/FO) to phase III (AF/AO), as shown in Ref. [50], but the Néel order persists in both of them and manifests itself in the two-spin correlation,  $\langle S_i^z S_{i+r}^z \rangle$ . For translational invariant and orthonormal linear combinations of the symmetry-broken Néel (AF) states,

$$\begin{aligned} |\Phi_1^{AF}\rangle &= |\uparrow\downarrow\uparrow\downarrow \cdots \uparrow\downarrow\rangle, \\ |\Phi_2^{AF}\rangle &= |\downarrow\uparrow\downarrow\uparrow \cdots \downarrow\uparrow\rangle, \end{aligned} \quad (3.17)$$

there are spin  $\langle S_i^z S_{i+r}^z \rangle = (-1)^r/4$  and dimer  $D(r) = 0$  correlations (for  $r \neq 0$ ), while for dimer states  $|\Phi_1^{DIM}\rangle$  and  $|\Phi_2^{DIM}\rangle$ ,  $\langle S_i^z S_{i+r}^z \rangle = 0$  (for  $r \neq \pm 1$ ) and  $D(r) \neq 0$  (for  $r \neq 0$ ), see Fig. 3, respectively. These results reflect the long-range nature of the two types of order. The AF classical spin correlations (3.17) are replaced by a power law for the AF spin  $S = 1/2$  chain in the thermodynamic limit,

$$\langle \vec{S}_i \cdot \vec{S}_{i+r} \rangle \sim (-1)^r \frac{\sqrt{\ln|r|}}{|r|}, \quad (3.18)$$

which is equivalently revealed by the structure factors  $S^{zz}(k)$  and  $T^{zz}(k)$  defined by Eqs. (3.1) and (3.2).

#### IV. ENTANGLEMENT IN THE GROUND STATES

##### A. The anisotropic orbital interactions ( $0 < \Delta \leq 1$ )

When  $\Delta = 0$ , there is no dynamics in the orbital sector, and the orbital structure factor is dominated by a single mode which follows from the  $\mathbb{Z}_2$  symmetry [50]. This changes when  $0 < \Delta \leq 1$  and the quantum fluctuations in the orbital sector contribute. In order to understand the modifications of the phase diagram in the entire interval  $0 < \Delta \leq 1$ , we select  $\Delta = 0.5$  and study the longitudinal equal-time spin/orbital structure factor, defined for a ring of length  $L$  in Eqs. (3.1) and (3.2).

The most important change at finite  $\Delta$  occurs for the phase transition between phases V and III (AF/AO) which becomes continuous for fixed  $y$  and decreasing  $x$ , with a gradual change of spin correlations from the alternating singlets to an AF order along the chain [50]. Here we discuss in more detail the intermediate case of  $\Delta = 0.5$ . First we address the phases with uniform spin-orbital order. The spin structure factors has distinct peaks at  $k = 0$  for FM order and at  $k = \pi$  for AF order. Similarly, one finds a maximum of the orbital structure factor  $T^{zz}(k)$  at  $k = 0$  for FO order and at  $k = \pi$  for AO order. These structure factors complement one another

and one finds that the spin correlations are somewhat weaker due to stronger spin fluctuations, while the orbital fluctuations are moderate at this value of  $\Delta = 0.5$ .

The dimerised phase V is characterized by a remarkably different behavior, see Figs. 4(c) and 4(d). Phase V, found at the  $E$  point in Fig. 5, has spin dimers accompanied by an orbital pattern with the periodicity of four sites, see Fig. 2(a). Spin correlations give a sharp maximum of  $S^{zz}(k)$  at  $k = \pi$  as for AF states, while two symmetric peaks of  $T^{zz}(k)$  at  $k = \pi/2$  and  $k = 3\pi/2$  indicate quadrupling of the unit cell in the orbital channel. When the model evolves towards the  $SU(2) \otimes SU(2)$  limit with increasing  $\Delta$ , one expects also a similar phase VI with interchanged role of spin and orbital correlations. Indeed, this complementary phase emerges already at small  $\Delta > 0$  and is identified by the respective structure factors shown also in Figs. 4(c) and 4(d).

The above analysis of the structure factors demonstrates that the phase diagram found for  $\Delta = 0.5$  contains six distinct phases, see Fig. 5. The quantum phase transitions at the boarder lines I-V and II-V are of first order. The phase transition between phases III (AF/AO) and V is a first order transition only for  $\Delta = 0$ , and here this transition is continuous [84]. As described above, phase VI emerges at finite  $\Delta$  but is still quite narrow in the phase diagram of Fig. 5. Also the phase transition

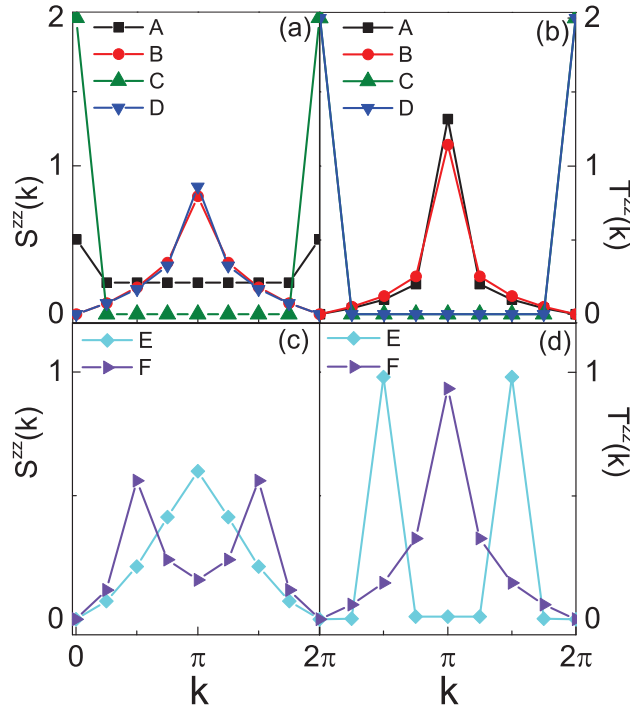


FIG. 4. (Color online) The spin  $S^{zz}(k)$  (a,c), and orbital  $T^{zz}(k)$  (b,d) structure factors obtained for the selected points shown in the phase diagram of the anisotropic spin-orbital  $SU(2) \otimes XXZ$  model, see Fig. 5: (a,b)  $A$ ,  $B$ ,  $C$  and  $D$  in phases I-IV, and (c,d)  $E$  and  $F$  in phases V and VI. Parameters:  $\Delta = 0.5$  and  $L = 8$  sites.

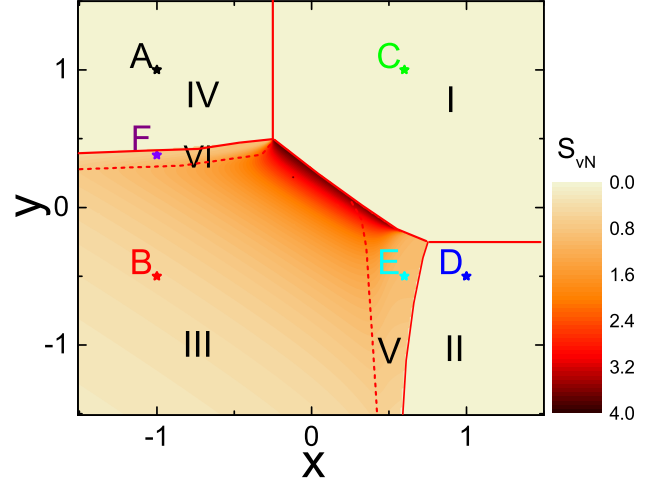


FIG. 5. (Color online) Phase diagram in the  $(x, y)$  plane and spin-orbital entanglement  $S_{vN}^0$  (1.1) (right scale) in different phases (indicated by color intensity) of the anisotropic spin-orbital  $SU(2) \otimes XXZ$  model (2.1) with  $\Delta = 0.5$ , obtained for a ring of  $L = 8$  sites. Phases I-IV correspond to FM/FO, AF/FO, AF/AO, FF/AO order in spin-orbital sectors. Orbitals (spins) follow a quadrupled pattern accompanied by spin (orbital) dimer correlations in phase V (VI). Six labeled points are:  $A = (-1, 1)$ ,  $B = (-1, -0.5)$ ,  $C = (0.5, 1)$ ,  $D = (0.5, -0.5)$ ,  $E = (1, -0.5)$ , and  $F = (-1, 0.38)$  — they are used to investigate spin and orbital structure factors in different phases, see Fig. 4. The phase boundaries, determined by the dominant modes of structure factors are shown by solid (dashed) lines for the first (second) order quantum phase transitions.

from phase III to phase VI is continuous. We have verified that due to the short-range nature of spin-orbital correlations, the size  $L = 12$  is sufficient as the phase boundaries are here almost the same as for the ring of  $L = 8$  sites.

TABLE I. The spin-orbital configurations, momenta  $k$ , the total spin  $S^z$  and orbital  $T^z$  quantum numbers of the ground states I-VI found for the anisotropic  $SU(2) \otimes XXZ$  model at  $\Delta < 1$ . All states in these subspaces are nondegenerate ( $d = 1$ ), but in case of  $S^z = L/2$  there are  $L + 1$  degenerate states for total  $S = L/2$ , and for  $T^z = L/2$  and  $\Delta < 1$  an equivalent state for  $-$  orbitals has  $T^z = -L/2$ . At  $\Delta = 0$  phase VI is absent and the ground state degeneracy of phase V changes to  $d = 4$  corresponding to momenta  $k = 0, \pm\pi/2, \pi$ .

phase	spin state	orbital state	$k$	$S^z$	$T^z$
I	$\uparrow\uparrow\uparrow\uparrow\uparrow\uparrow$	$++++++$	0	$L/2$	$L/2$
II	$\uparrow\downarrow\uparrow\downarrow\uparrow\downarrow$	$++++++$	0	0	$L/2$
III	$\uparrow\downarrow\uparrow\downarrow\uparrow\downarrow$	$+ - + - + -$	0	0	0
IV	$\uparrow\uparrow\uparrow\uparrow\uparrow\uparrow$	$+ - + - + -$	0	$L/2$	0
V	$(S = 0)$ singlets	$+ - - + + - + -$	0	0	0
VI	$\uparrow\downarrow\uparrow\downarrow\uparrow\downarrow$	$(T = 0)$ singlets	0	0	0

The spin-orbital phases I-VI found at  $\Delta > 0$  are summarized in Table I. Phases I-IV have polarized or alternating spin and orbital components, combined in all possible ways into phases: FM/FO, AF/FO, AF/AO, and FM/AO. Phases with either  $S^z = L/2$  or  $T^z = L/2$  (FM or FO) have of course also degeneracy with respect to other possible values of  $S^z$  or  $T^z$  (the latter only at  $\Delta = 1$  when  $T$  is also a good quantum number). In addition, there are two phases with dimer orbital (phase V) or dimer spin (phase VI) correlations. It is remarkable that these two phases survive in the isotropic model at  $\Delta = 1$ , see Sec. IV B.

For  $\Delta > 0$  also phase III is characterized by finite SOE, and it expands to higher values of  $y$  along vertical lines for fixed  $x < -0.25$ . Indeed, the onset of entangled region in the phase diagram of Fig. 5 moves to higher values of  $y$  with increasing  $\Delta$ , see Fig. 6. At  $\Delta = 0.25$  the entanglement entropy  $\mathcal{S}_{\text{vN}}^0$  develops a narrow peak with a maximum at  $y \simeq 0.15$ . This maximum broadens up and moves somewhat to the right (to higher  $y$ ) when the orbital fluctuations increase with increasing  $\Delta$  towards the isotropic  $\text{SU}(2) \otimes \text{SU}(2)$  model. A sharp increase of the entropy to  $\mathcal{S}_{\text{vN}}^0 = 1$ , visible in all the curves shown in Fig. 6, signals the SOE in phase VI which increases with increasing  $\Delta$ . This large SOE can develop because phase VI is similar to phase V — it does not break translation invariance of the model and different spin-orbital configurations contribute simultaneously.

To detect SOE we employ here not only the vNE,  $\mathcal{S}_{\text{vN}}^0$  Eq. (1.1), but also a direct measure by the spin-orbital

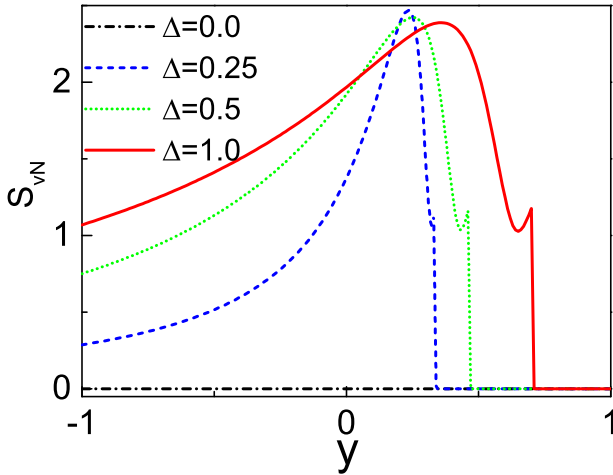


FIG. 6. (Color online) Spin-orbital entanglement entropy  $\mathcal{S}_{\text{vN}}^0$  (2.1) in the ground state of the spin-orbital model (2.1) as a function of  $y$  for selected values of  $\Delta$ . The onset of phase VI is detected at  $\Delta > 0$  by a step-like increase of entropy to  $\mathcal{S}_{\text{vN}}^0 = 1$ . Parameters:  $x = -0.5$  and  $L = 8$ .

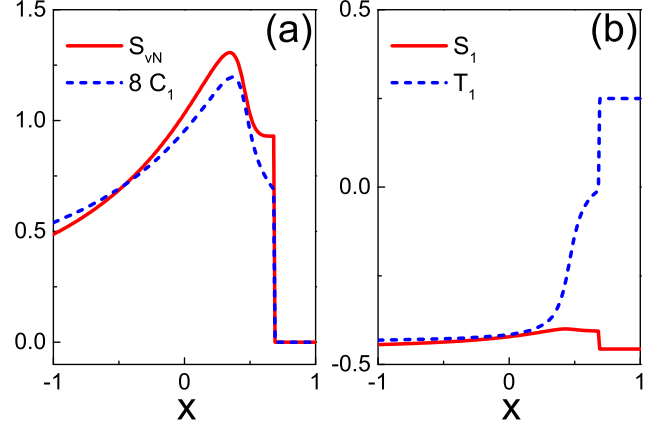


FIG. 7. (Color online) The onset of phase V and its gradual change into phase III with decreasing  $x$  in the ground state of the spin-orbital model (2.1): (a) spin-orbital entanglement entropy  $\mathcal{S}_{\text{vN}}^0$  (1.1) and the spin-orbital correlation function  $C_1$  (4.1); (b) spin  $S_1$  (4.2) and orbital  $T_1$  (4.3) correlation functions. The onset of phase V is signaled by a step-like increase of the entropy to  $\mathcal{S}_{\text{vN}}^0 = 1$ . Parameters:  $\Delta = 0.5$ ,  $y = -0.5$  and  $L = 8$ .

correlation function on a bond [19],

$$C_1 \equiv \frac{1}{L} \sum_{i=1}^L \left[ \langle \vec{S}_i \cdot \vec{S}_{i+1} \rangle \langle \vec{T}_i \cdot \vec{T}_{i+1} \rangle - \langle \vec{S}_i \cdot \vec{S}_{i+1} \rangle \langle \vec{T}_i \cdot \vec{T}_{i+1} \rangle \right], \quad (4.1)$$

and we compare it with the conventional intersite spin- and orbital correlation functions:

$$S_1 \equiv \frac{1}{L} \sum_{i=1}^L \langle \vec{S}_i \cdot \vec{S}_{i+1} \rangle, \quad (4.2)$$

$$T_1 \equiv \frac{1}{L} \sum_{i=1}^L \langle \vec{T}_i \cdot \vec{T}_{i+1} \rangle. \quad (4.3)$$

The above general expressions imply averaging over the exact (translation invariant) ground state found from Lanczos diagonalization of a ring of length  $L$ . While  $S_1$  (4.2) and  $T_1$  (4.3) correlations indicate the tendency towards particular spin and orbital order,  $C_1$  (4.1) quantifies the SOE — if  $C_1 \neq 0$  spin and orbital degrees of freedom are entangled and the mean-field decoupling cannot be applied in Eq. (2.1) as it generates systematic errors.

To gain a better insight into the nature of a phase transition between phases II (AF/FO) and V and between V and III (AF/AO) which occur for decreasing  $x$  at a fixed  $y < -1/4$ , we study SOE vNE  $\mathcal{S}_{\text{vN}}^0$ , joint spin-orbital  $C_1$  (4.1), and individual spin  $S_1$  (4.2) and orbital  $T_1$  (4.3) correlations in Fig. 7. Both  $\mathcal{S}_{\text{vN}}^0$  and  $C_1$  show a very similar behavior with a maximum within phase V, see Fig. 7(a). The SOE is lower in phase III than in phase V, i.e., below  $x \simeq -0.25$ , and decreases further with decreasing  $x$ . These two phases have rather similar



spin correlations  $S_1$ , but orbital correlations  $T_1$  are similar to spin ones only within phase III (AF/AO); above  $x \simeq -0.25$  they vary fast within phase V and almost disappear ( $T_1 \simeq 0$ ) near the transition point to phase II (AF/FO), see Fig. 7(b).

### B. Isotropic spin-orbital $SU(2) \otimes SU(2)$ model

The phase diagram of the isotropic  $SU(2) \otimes SU(2)$  model (Fig. 8) includes the same six phases as the one obtained at  $\Delta = 0.5$  (Fig. 5), with spin-orbital correlations explained in Table I. The main differences to the phase diagram at  $\Delta = 0.5$  is a somewhat reduced stability range of phase IV (FM/AO), and also phase II (AF/FO), both destabilized by enhanced spin-orbital fluctuations in and around phase III (AF/AO). The range of entangled ground states is broad and includes phase III as well as phases V and VI on its both sides. The phase transitions from phase I where all quantum fluctuations are absent to either phase II or IV are given by straight lines and may be determined using mean-field approach.

It is quite unexpected that the dimerised phases V and VI survive in the phase diagram of the isotropic  $SU(2) \otimes SU(2)$  model at  $\Delta = 1.0$ , see Fig. 8. These two phases emerge in between a disentangled phase II and III in the case of phase V, and similarly between phases IV and III in the case of phase VI, and are stabilized by robust quadrupling of orbital or spin correlations which was overlooked before [43]. This is not so surprising as one expects that isotropic spin-orbital interactions would lead instead to uniform phases only. In each case the effective exchange interaction changes sign in one (either spin or orbital) channel which resembles the mechanism of exotic magnetic order found in the Kugel-Khomskii model [85].

The phases V and VI emerge by the same mechanism as phase V for the Ising orbital interactions, see Sec. III. In the isotropic model this phase and phase VI with complementary spin-orbital correlations occur in a symmetric way with respect to the  $x = y$  line, see Fig. 8. Orbital correlations in the case of phase V (spin correlations in the case of phase VI) change gradually towards FO (FM) order in phase II (IV) with increasing  $x$  ( $y$ ). The quadrupling of the unit cell seen in both phases in such correlations, shown in Fig. 9, may be seen as a precursor of this transition. Both phases are stable only in a rather narrow range and disappear for  $y \rightarrow -\infty$  or  $x \rightarrow -\infty$ , respectively, as presented in the inset of Fig. 8 for phase VI. The spin-orbital interactions and the mechanism stabilizing these phases are different from spin-Peierls and orbital-Peierls mechanisms in the 1D  $SU(2) \otimes SU(2)$  spin-orbital model with positive exchange ( $J = -1$ ) [63]. We emphasize that the present mechanism of dimerization is effective only in one (spin or orbital) channel and thus it is also distinct from the spin-orbital dimerization in a FM chain found at finite temperature [86].

A characteristic feature of SOE in phase VI (and simi-

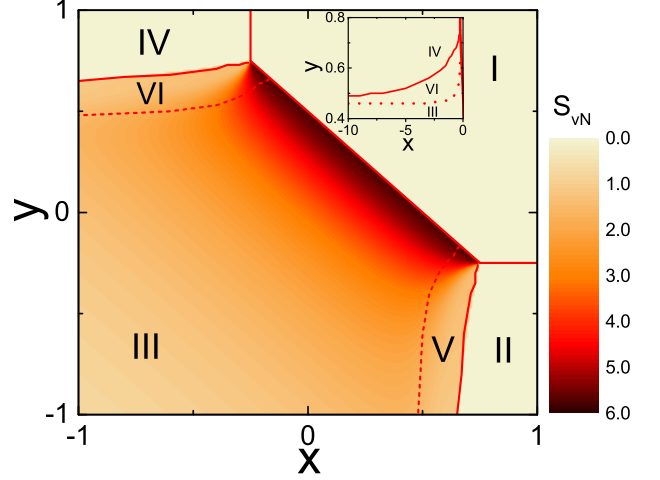


FIG. 8. (Color online) Phase diagram in the  $(x, y)$  plane and spin-orbital entanglement  $S_{vN}^0$  (1.1) (right scale) in the ground state of the isotropic spin-orbital  $SU(2) \otimes SU(2)$  model (2.1) with  $\Delta = 1.0$  obtained for a ring of  $L = 12$  sites. Phases I-IV correspond to FM/FO, AF/FO, AF/AO, FM/AO order in spin-orbital sectors. Orbitals (spins) follow a quadrupled pattern accompanied by spin (orbital) dimer correlations in phase V (VI). The phase boundaries determined by dominant modes of structure factors, shown by solid (dashed) lines, are of first (second) order. Inset shows the extended range of phase VI which separates phases IV and III for  $-10 < x < 0$ .

lar in phase V) is a competition between the spin (orbital) quadrupling correlations along the chain which support orbital (spin) singlets, with the AF/AO order character-

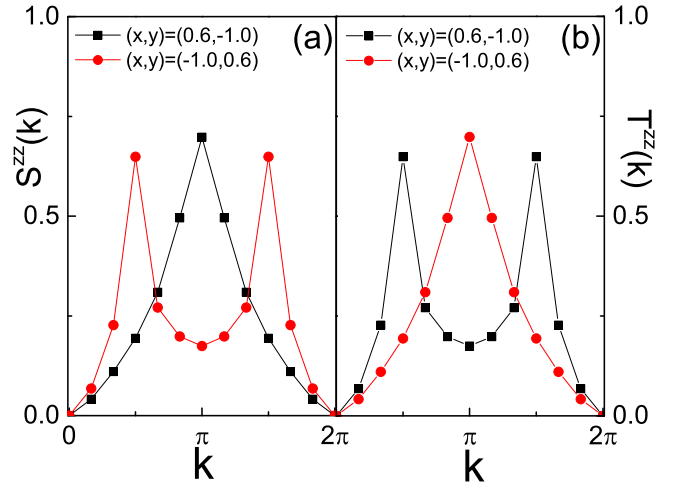


FIG. 9. (Color online) The structure factors obtained for a spin-orbital ring Eq. (2.1) of  $L = 8$  sites in the full Hilbert space at  $\Delta = 1.0$ : (a) spin  $S^{zz}(k)$ , and (b) orbital  $T^{zz}(k)$ . The points  $(0.6, -1.0)$  (filled squares) and  $(-1.0, 0.6)$  (filled circles) correspond to phase V and VI, see Fig. 8.

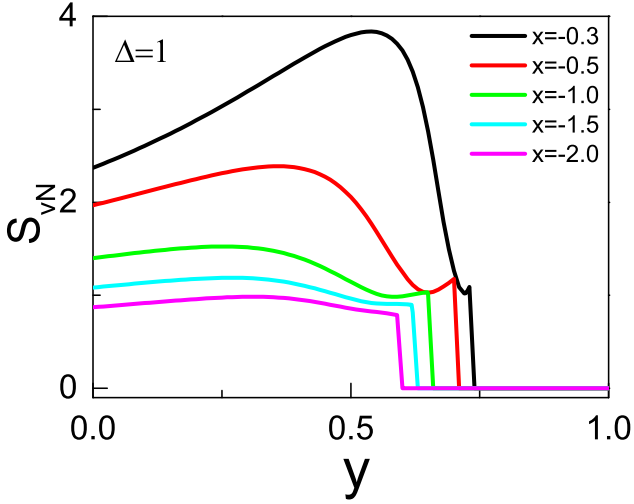


FIG. 10. (Color online) Spin-orbital entanglement entropy  $S_{\text{vN}}^0$  in the ground state of the  $\text{SU}(2) \otimes \text{SU}(2)$  spin-orbital model (2.1) as a function of  $y$  for representative values of  $x \in [-2.0, -0.3]$ . The onset of phase VI at decreasing  $y$  is detected by a step-like increase of entropy at the IV-VI phase transition.

istic of phase III (AF/AO). For  $x \in [-1.0, -0.3]$  the vNE  $S_{\text{vN}}^0$  increases discontinuously at the phase transition IV-VI, next drops somewhat and next increases further, see Fig. 10. It exhibits a broad maximum, moving to lower values of  $y$  with decreasing  $x$ . This behavior shows that two phases (VI and III) compete in this regime. For still lower values of  $x$  the SOE entropy is smaller and almost constant when  $y$  decreases deeply into phase III.

### C. Entanglement in the $\text{SU}(2) \otimes \text{SU}(2)$ models

The ground state obtained in the present spin-orbital  $\text{SU}(2) \otimes \text{SU}(2)$  model for phase III (AF/AO) is distinct from the one found for positive coupling constant, i.e.,  $J = -1$  in Eq. (2.1). We elucidate this difference by studying both models along the symmetry line  $x = y$  in the phase diagram. Phase I (FM/FO) is found in the present case for  $x = y > 1/4$ , while in the case of positive coupling constant it becomes the ground state for  $x = y < -1/4$  [61].

First we consider SOE detected by the vNE  $S_{\text{vN}}^0$  Eq. (1.1), and by the joint spin-orbital correlation function  $C_1$  (4.1), see Fig. 11. To understand better the transition from phase I to phase III, we consider the correlation functions along the symmetry line  $x = y$ . Phase I with FM/FO order is disentangled in both cases. At the quantum phase transition to phase III, signalled by a rapid increase of both  $S_{\text{vN}}^0$  and  $8|C_1|$ , we observe that the entropy reaches the highest value at the onset of phase III, and then decreases when  $x$  decreases and one moves deeper into the entangled phase III. In the present model (2.1) one finds  $C_1 > 0$  which is imposed by the negative

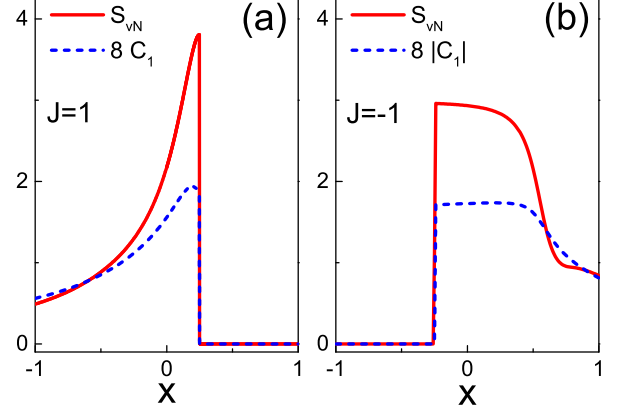


FIG. 11. (Color online) von Neumann entropy  $S_{\text{vN}}^0$  (1.1) and joint spin-orbital bond correlation  $C_1$  (4.1) as obtained in the  $\text{SU}(2) \otimes \text{SU}(2)$  model (2.1) along the symmetry  $x = y$  line in the phase diagram with the ring of  $L = 8$  sites for: (a) the model with negative coupling  $-J = -1$  [43], and (b) the model with positive coupling  $-J = 1$  constant [56].

coupling constant. The entropy maximum and also the maximum of  $8C_1$  are sharp indeed and signal the onset of phase III, see Fig. 11(a). The model with a positive coupling constant behaves differently — here the joint spin-orbital correlations are negative  $C_1 < 0$ , and both  $S_{\text{vN}}^0$  and  $8|C_1|$  have flat maxima in a range of  $x$  and only at  $x \simeq 0.5$  both drop rapidly. This large SOE for  $x \in [-0.25, 0.5]$  indicates a spin-orbital liquid phase which forms near the  $\text{SU}(4)$  point  $x = y = 1/4$  [61]. Only at  $x > 0.5$  the strong spin-orbital fluctuations are weakened when phase III is approached and SOE decreases.

A special feature of the present  $\text{SU}(2) \otimes \text{SU}(2)$  spin-orbital model is a very distinct behavior along the I-III phase transition line  $x + y = 1/2$ , see Fig. 8. The ground state energy of phase I (FM/FO) in which quantum fluctuations are absent,  $E^0 = -J(1/4 + x)^2$ , is found by taking exact classical values of spin (4.2) and orbital (4.3) correlations on the bonds,  $S_1 = T_1 = 1/4$ . The energy decreases when the transition at  $x = 1/4$  is approached. On the contrary, coming from the other side it is not allowed to assume classical correlations,  $S_1 = T_1 = -1/4$ , as then the Hamiltonian would vanish at the transition. In fact the energy  $E_0 = -J/4$  can be also obtained mainly from enhanced joint spin-orbital correlations,  $\langle (\vec{S}_j \cdot \vec{S}_{j+1})(\vec{T}_j \cdot \vec{T}_{j+1}) \rangle = 5/16$  and  $C_1 = 1/4$ , see Fig. 11. At the phase transition the spin and orbital correlations are *very weak*, i.e.,  $S_1 = T_1 \simeq -1/8$ . This is a very peculiar situation as joint spin-orbital correlations cannot be factorized and damp to a large extent individual spin and orbital correlations.

A qualitatively different nature of the SOE in both  $\text{SU}(2) \otimes \text{SU}(2)$  models is also captured by its effect on the individual spin (orbital) correlations, see Fig. 12. In the present model (2.1) with  $J = 1$ ,  $C_1 > 0$  damps individ-

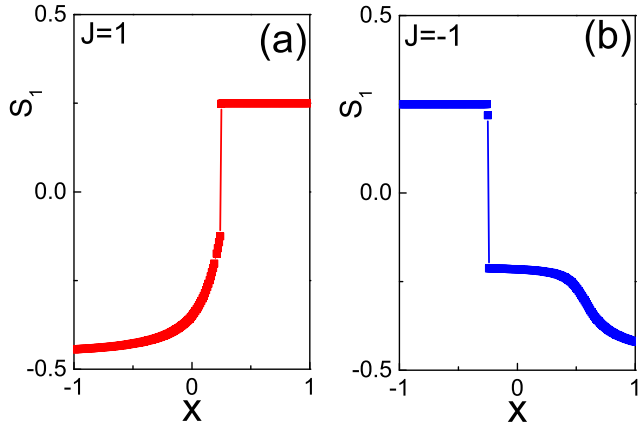


FIG. 12. (Color online) Spin  $S_1$  (4.2) and orbital  $T_1$  (4.3) ( $T_1 = S_1$ ) bond correlations as obtained in the  $SU(2) \otimes SU(2)$  model (2.1) along the symmetry line  $x = y$  in the phase diagram with the ring of  $L = 8$  sites for: (a) the model with negative exchange  $J = 1$  [43], and (b) the model with positive exchange  $J = -1$  [56].

ual spin and orbital fluctuations near the quantum phase transition stronger than in the case of positive coupling ( $J = -1$ ), cf. Figs. 12(a) and 12(b). However, the joint fluctuations  $C_1$  decrease fast when  $J = 1$ , while they are robust in the spin liquid phase for  $J = -1$  when  $x \in [0.25, 0.50]$ . At  $x = 0$  one finds  $S_1 = T_1 \simeq -0.37$ , already much below the value of  $S_1 = T_1 \simeq -0.22$  found for  $J = -1$ . The spin  $S_1$  and orbital  $T_1$  correlations become similar in both phases deeply within phase III, as found by comparing these values at  $x = -1$  for  $J = 1$

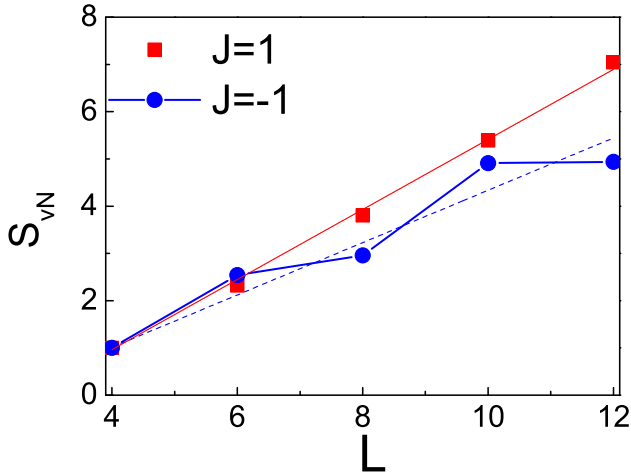


FIG. 13. (Color online) von Neumann entropy  $S_{vN}^0$  (1.1) obtained in the isotropic  $SU(2) \otimes SU(2)$  model (2.1) at the maximum seen in Fig. 11(a) at  $x = y = 0.249$  (squares) and at  $J = -1$  at  $x = y = -0.249$  (circles), i.e., at the onset of phase III, both for rings of  $L = 4, 6, \dots, 12$  sites and the linear fits to the data (dashed lines).

and at  $x = 1$  for  $J = -1$ . Here SOE is weak because spins and orbitals fluctuate almost independently.

The sharp peak of  $S_{vN}^0$  found near the phase transition for  $J = 1$  is rather unusual, see Fig. 11(a). In this regime of parameters the ground state energy  $E_0$  is lowered by positive joint spin-orbital correlations  $C_1$ , while negative  $S_1 = T_1 \simeq -1/8$  [Fig. 12(a)] increase it somewhat. Large vNE  $S_{vN}^0$  is found near the phase transition for rings of even length, starting from  $S_{vN}^0 \simeq 1$  for  $L = 4$ . It is remarkable that the vNE at the maximum scales with system size  $L$ , see Fig. 13. This behavior is unique and proves that SOE which takes place at every bond is extensive and extends here over the entire ring. The model with positive coupling constant,  $J = -1$ , has also a similar linear scaling,  $S_{vN}^0 \propto L$ , but the entropy is smaller and systematic fluctuations between the rings of length of  $4n$  and  $4n+2$  sites, seen in Fig. 13, are distinct and indicate a crucial role played here by global  $SU(4)$  singlets.

## V. ENTANGLED ELEMENTARY EXCITATIONS: FM/FO ORDER

### A. Analytic approach

When the ground state is disentangled, SOE is generated locally in excited states [87] and would not scale linearly with system size. Indeed, we analyzed the low-energy excitations of the disentangled FM/FO phase in the 1D  $SU(2) \otimes SU(2)$  spin-orbital model in Ref. [43] and found a much weaker dependence on system size. We investigated the SOE for spin-orbital bound states (BSs) and spin-orbital exciton (SOEX) state and found a logarithmic scaling, while the entropy saturates for other separable (trivial) spin-orbital excitations. One finds that the vNE is controlled by the spin-orbital correlation length  $\xi$  and decays logarithmically with ring length  $L$ .

Here we consider again the FM/FO disentangled ground state  $|0\rangle$ , obtained for the anisotropic spin-orbital  $SU(2) \otimes XXZ$  model with the exactly known ground state energy  $E^0$ ,

$$H|0\rangle = E^0|0\rangle. \quad (5.1)$$

Using equation of motion method one finds spin (magnon) excitations with dispersion

$$\omega_S(Q) = \left(\frac{1}{4} + y\right) (1 - \cos Q), \quad (5.2)$$

and orbital (orbiton) excitations [88],

$$\omega_T(Q) = \left(\frac{1}{4} + x\right) (1 - \Delta \cos Q). \quad (5.3)$$

The spin-orbital continuum is given by

$$\Omega(Q, q) = \omega_S\left(\frac{Q}{2} - q\right) + \omega_T\left(\frac{Q}{2} + q\right). \quad (5.4)$$

Next, we consider the propagation of a magnon-orbital pair excitation along the FM/FO chain, by exciting simultaneously a single spin and a single orbital. The translation symmetry imposes that total momentum  $Q = 2m\pi/L$  (for  $m = 0, \dots, L-1$ ) is conserved during scattering. The scattering of magnon and orbital with initial (final) momenta  $\{\frac{Q}{2}-q, \frac{Q}{2}+q\}$  ( $\{\frac{Q}{2}-q', \frac{Q}{2}+q'\}$ ) and the total momentum  $Q$  is represented by the Green's function [89],

$$G(Q, \omega) = \frac{1}{L} \sum_{q, q'} \langle \langle S_{\frac{Q}{2}-q'}^+ T_{\frac{Q}{2}+q'}^+ | S_{\frac{Q}{2}-q}^- T_{\frac{Q}{2}+q}^- \rangle \rangle, \quad (5.5)$$

for a combined spin ( $S_{\frac{Q}{2}-q}^-$ ) and orbital ( $T_{\frac{Q}{2}+q}^-$ ) excitation. The analytical form reads

$$G(Q, \omega) = G^0(Q, \omega) + \Pi(Q, \omega), \quad (5.6)$$

$$\begin{aligned} \Pi(Q, \omega) = & -\frac{2(1+\Delta) + (1-\Delta^2)F_{ss}(Q, \omega)}{4[1+\Lambda(Q, \omega)]} H_{cc}^2(Q, \omega) \\ & -\frac{2(1-\Delta) + (1-\Delta^2)F_{cc}(Q, \omega)}{4[1+\Lambda(Q, \omega)]} H_{ss}^2(Q, \omega) \\ & +\frac{(1-\Delta^2)F_{sc}(Q, \omega)}{2[1+\Lambda(Q, \omega)]} H_{cc}(Q, \omega) H_{ss}(Q, \omega), \end{aligned} \quad (5.7)$$

where the noninteracting Green's function is given by

$$G^0(Q, \omega) = \frac{1}{L} \sum_q G_{qq}^0(Q, \omega), \quad (5.8)$$

$$G_{qq}^0(Q, \omega) = \frac{1}{\omega - \Omega(Q, q)}, \quad (5.9)$$

and

$$H_{cc}(Q, \omega) = \frac{1}{L} \sum_q \left( \cos \frac{Q}{2} - \cos q \right) G_{qq}^0(Q, \omega), \quad (5.10)$$

$$H_{ss}(Q, \omega) = \frac{1}{L} \sum_q \left( \sin \frac{Q}{2} - \sin q \right) G_{qq}^0(Q, \omega). \quad (5.11)$$

One finds the denominator in  $\Pi(Q, \omega)$  (5.7),

$$\begin{aligned} & 1 + \Lambda(Q, \omega) \\ = & \left[ 1 + \frac{1}{2}(1+\Delta)F_{cc}(Q, \omega) \right] \left[ 1 + \frac{1}{2}(1-\Delta)F_{ss}(Q, \omega) \right] \\ & - \frac{1}{4}(1-\Delta^2)F_{sc}^2(Q, \omega), \end{aligned} \quad (5.12)$$

with

$$F_{cc}(Q, \omega) = \frac{1}{L} \sum_q \frac{(\cos \frac{Q}{2} - \cos q)^2}{\omega - \Omega(Q, q)}, \quad (5.13)$$

$$F_{ss}(Q, \omega) = \frac{1}{L} \sum_q \frac{(\sin \frac{Q}{2} - \sin q)^2}{\omega - \Omega(Q, q)}, \quad (5.14)$$

$$F_{sc}(Q, \omega) = \frac{1}{L} \sum_q \frac{(\sin \frac{Q}{2} - \sin q)(\cos \frac{Q}{2} - \cos q)}{\omega - \Omega(Q, q)}. \quad (5.15)$$

Here we define a phase  $\delta \in [0, 2\pi]$  which quantifies the difference of dynamic properties of magnon and orbital excitations throughout the Brillouin zone in the form

$$\tan \delta = \frac{(4y+1) - (4x+1)\Delta}{(4y+1) + (4x+1)\Delta} \tan \left( \frac{Q}{2} \right). \quad (5.16)$$

For the symmetry line  $x = y$  Eq. (5.16) greatly simplifies for the isotropic model at  $\Delta = 1$  and gives  $\delta(Q) = 0$ , which has been studied in Ref. [43]. Also, a quantity describes the position relative to the continuum is given by

$$a(Q, \omega) = \frac{\omega - (x + y + \frac{1}{2})}{b(Q)}, \quad (5.17)$$

with

$$\begin{aligned} b(Q) = & \left[ \left( x + \frac{1}{4} \right)^2 \Delta^2 + \left( y + \frac{1}{4} \right)^2 \right. \\ & \left. + 2\Delta \left( x + \frac{1}{4} \right) \left( y + \frac{1}{4} \right) \cos Q \right]^{1/2}. \end{aligned} \quad (5.18)$$

The excitations at the top and at the bottom of the continuum correspond to  $a(Q, \omega) = 1$  and  $-1$ , respectively. In the noninteracting case, we have the imaginary and real parts of Eq. (5.6),

$$\Im G^0(Q, \omega) = -\frac{\theta(1 - |a(Q, \omega)|)}{b(Q)\sqrt{1 - a^2(Q, \omega)}}, \quad (5.19)$$

$$\begin{aligned} \Re G^0(Q, \omega) = & \frac{\theta(a(Q, \omega) - 1)}{b(Q)\sqrt{a^2(Q, \omega) - 1}} \\ & - \frac{\theta(-1 - a(Q, \omega))}{b(Q)\sqrt{a^2(Q, \omega) - 1}}, \end{aligned} \quad (5.20)$$

where  $\theta(x)$  is Heaviside step function whose value is zero for negative argument and 1 for nonnegative argument. The frequency dependence of the imaginary part exhibits square-root singularities in Eq. (5.19) at the bottom and at the top of the continuum [90].

## B. Numerical studies

We note that the inclusion of the spin-orbital attraction will smear out the singularities by Eq. (5.6) since a more pronounced divergence of the numerator than the denominator occurs when  $a(Q, \omega) \rightarrow \pm 1$ , and they cancel each other, i.e.,  $\Im G(Q, \omega) = 0$ . Furthermore, the poles of  $G(Q, \omega)$  are determined by

$$1 + \Lambda(Q, \omega) = 0. \quad (5.21)$$

Our analysis shows that for given  $Q$  most the real solutions of Eq. (5.21) are interspersed within the continuum, but these modes are unstable to two free waves. However, a small number of solutions may lie well below the continuum. To investigate the spectra we begin with



the asymmetric  $SU(2) \otimes XXZ$  model. As it is shown in Fig. 14, the attractive interactions shift spin-orbital BSs outside the continuum [91–93]. The binding energy approaches zero for the isotropic  $SU(2) \otimes SU(2)$  model, but is finite for anisotropic  $SU(2) \otimes XXZ$  model due to a gap in the orbital excitation spectrum, and the small- $q$  behavior of the binding energy reveals that the BSs appear for arbitrarily small wave number.

The BSs can be also obtained by the equation of motion method for a spin-orbital joint excitation,  $S_m^- T_{m+l}^- |0\rangle$ . The collective mode follows from Eq. (5.21). Such a collective spin-orbital excitation (bound state) involves spin and orbital flips at many sites and can be written as follows,

$$\begin{aligned} |\Psi(Q)\rangle &= \frac{1}{\sqrt{L}} \sum_{m,l} a_l(Q) e^{iQm} S_m^- T_{m+l}^- |0\rangle \\ &= \sum_q a_q S_{\frac{Q}{2}-q}^- T_{\frac{Q}{2}+q}^- |0\rangle, \end{aligned} \quad (5.22)$$

with the coefficients

$$a_q = \frac{1}{\sqrt{L}} \sum_l a_l(Q) e^{-i(\frac{Q}{2}-q)l}. \quad (5.23)$$

The correlation length  $\xi \equiv \sum_l l |a_l|^2$  defines the average size of spin-orbital BSs or excitons and is much smaller than the system size, i.e.,  $0 < \xi \ll L$ . The correlation length becomes extensive for a trivial continuum state, as shown in Fig. 15. The analytic solution of this equation is tedious but straightforward. The dispersion of the collective excitation,  $\omega_{BS}(Q)$ , can be analyzed in a simple way at some special points, including  $Q = 0$  and  $Q = \pi$ .

In the isotropic model (at  $\Delta = 1$ ), Eq. (5.21) reduces to  $1 + F_{cc}(Q, \omega) = 0$ . In this case there is at most one solution for every  $Q$  [43]. Nevertheless, the anisotropic orbital coupling will induce more branches in part of Brillouin zone (see Fig. 14). When  $\Delta < 1$  and  $Q = 0$ ,  $F_{sc}(0, \omega) = 0$  and then Eq. (5.21) reduces to

$$1 + \frac{1}{2}(1 + \Delta)F_{cc}(0, \omega) = 0, \quad (5.24)$$

or

$$1 + \frac{1}{2}(1 - \Delta)F_{ss}(0, \omega) = 0. \quad (5.25)$$

The solution that follows from Eq. (5.24) is given by

$$\begin{aligned} \omega_{BS,1}(0) &= \frac{(\alpha + 3\beta)^2 - \sqrt{(\alpha - 17\beta)(\alpha - \beta)^3}}{8\beta} \\ &\quad + x(1 - \Delta) - 3\beta + \frac{1}{2}, \end{aligned} \quad (5.26)$$

where  $\alpha = (\Delta x + y)$ ,  $\beta = (1 + \Delta)/4$ . The instability of such a mode given by  $\omega_{BS,1}(0) = 0$  sets up the threshold of the FM/FO state separating it from the AF/AO state (phase III) [43, 92]. Moreover, the solution for Eq. (5.25) is given by

$$\omega_{BS,2}(0) = x + y - \frac{(\alpha + \beta)^2}{(1 - \Delta)} + \beta. \quad (5.27)$$

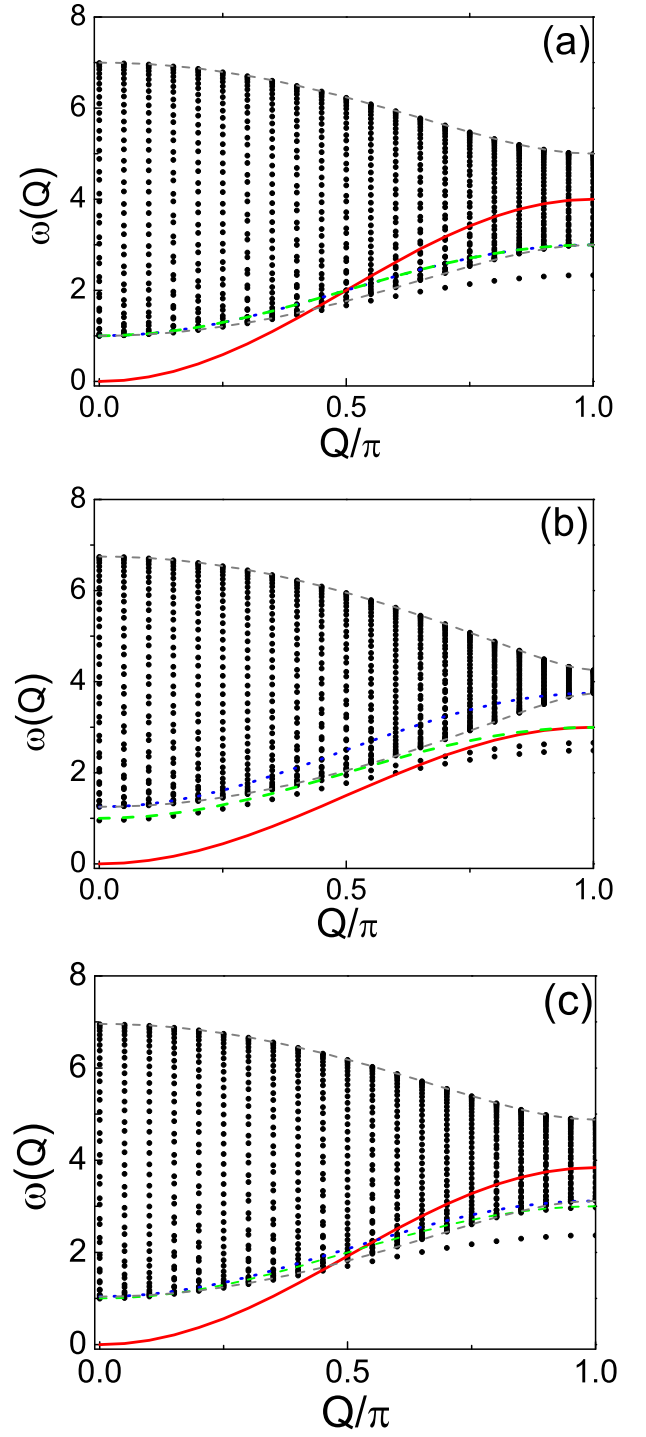


FIG. 14. (Color online) (a) Excitation spectra of a ring of  $L = 40$  sites for the spin-orbital  $SU(2) \otimes XXZ$  model with  $\Delta = 0.5$  as function of momentum  $Q$  at: (a)  $x = y = 1/4$ , (b)  $x = 0.375$ ,  $y = 0.125$ , and (c)  $x = 0.27$ ,  $y = 0.23$ . The dotted (blue), dashed (green) lines inside the spin-orbital continuum  $\Omega(Q, q)$  denote the orbital and SOEX excitations, i.e.,  $\omega_T(Q)$  and  $\omega_{SOEX}(Q)$ , respectively, that are degenerate. The (red) solid lines show spin excitations.

We find that when  $\alpha < (1 - 3\Delta)/4$ , both  $\omega_{BS,1}(0)$  and

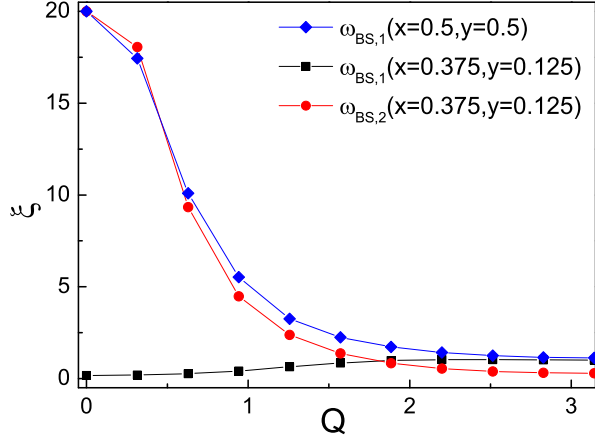


FIG. 15. (Color online) The correlation length  $\xi$  for increasing momentum  $Q$  as obtained for a ring of  $L = 80$  sites in the anisotropic  $SU(2) \otimes XXZ$  model with  $\Delta = 0.5$ .

$\omega_{BS,2}(0)$  exist, while only  $\omega_{BS,1}(0)$  survives when  $(1 + \Delta)/4 > \alpha > (1 - 3\Delta)/4$ . Finally, for  $\alpha > (1 + \Delta)/4$  no bound states exist.

When  $\Delta < 1$  and  $Q = \pi$ , one finds that  $F_{sc}(\pi, \omega) = 0$ . Analogously, Eq. (5.21) has two solutions,  $\omega_{BS,1}(\pi)$  and  $\omega_{BS,2}(\pi)$  when  $-(3 + \Delta)/4 < y - \Delta x < (1 - \Delta)/4$ , with explicit expressions for their energies:

$$\omega_{BS,1}(\pi) = x + y + \frac{1}{2} - \frac{1 + \Delta}{4} - \frac{[(y + \frac{1}{4}) - \Delta(x + \frac{1}{4})]^2}{1 + \Delta}, \quad (5.28)$$

$$\omega_{BS,2}(\pi) = x + y + \frac{1}{2} + \frac{\zeta - (2\gamma - 1 - \Delta)^{\frac{3}{2}} \sqrt{2\gamma - 9 + 9\Delta}}{8(\Delta - 1)}, \quad (5.29)$$

with

$$\gamma = (y + 1/4) - \Delta(x + 1/4), \quad \zeta = 3 + 4\gamma - 4\gamma^2 - 6\Delta - 4\gamma\Delta + 3\Delta^2. \quad (5.30)$$

When  $y - \Delta x < -(3 + \Delta)/4$  and  $(1 - \Delta)/4 < y - \Delta x < (3\Delta + 1)/4$ , only one  $\omega_{BS,1}(\pi)$  solution exists. In case of  $y - \Delta x = (1 - \Delta)/4$ ,  $\omega_{BS,2}(\pi)$  merges with lower boundary of the continuum.

### C. Propagating spin-orbital exciton states

Especially at the  $SU(4)$  symmetric point, i.e., at  $x = y = 1/4$ , spinon and orbion are strongly coupled to form a joint SOEX state inside the spin-orbital continuum across the whole Brillouin zone. Usually such an elementary spin-orbital excitation in the continuum is unstable and decays into a spinon and an orbion [38]. However, it is surprising that such a SOEX state propagates here as a undamped on-site spin-orbital excitation

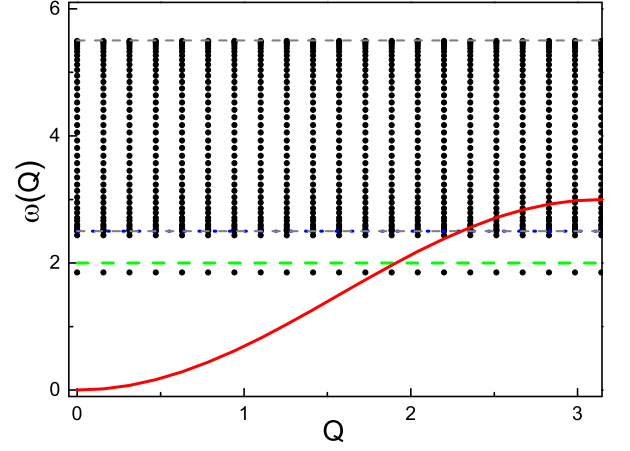


FIG. 16. (Color online) Excitation spectrum for the spin-orbital  $SU(2) \otimes \mathbb{Z}_2$  model (2.1) on a ring of  $L = 40$  sites. The dotted (blue) and dashed-dotted (gray) lines indicate the orbital excitation  $\omega_T(Q)$  and the lower boundary of the continuum  $\Omega_c(Q)$ ,  $\omega_c(Q)$  — both are degenerate. The dashed (green) and solid (red) lines denote the SOEX excitations  $\omega_{SOEX}(Q)$ , and spin excitations  $\omega_S(Q)$ . Parameters:  $\Delta = 0.0$ ,  $x = 0.375$ , and  $y = 0.125$ .

[88], e.g.  $S_l^- T_l^- |0\rangle$  at site  $l$ , within the spin-orbital continuum with  $\xi = 0$  (see Eq. (5.23)). It is straightforward to derive,

$$[H, S_l^- T_l^-] |0\rangle = [C_l(x, y) + D_l(x, y)] |0\rangle, \quad (5.31)$$

where

$$C_l(x, y) = (x + y) S_l^- T_l^- - \frac{\Delta}{4} (S_{l-1}^- T_{l-1}^- + S_{l+1}^- T_{l+1}^-), \quad (5.32)$$

$$D_l(x, y) = -\frac{1}{2} \left[ \Delta \left( x - \frac{1}{4} \right) (S_l^- T_{l-1}^- + S_l^- T_{l+1}^-) + \left( y - \frac{1}{4} \right) (S_{l-1}^- T_l^- + S_{l+1}^- T_l^-) \right].$$

The dissipative term  $D_l(x, y)$  vanishes when  $x = y = 1/4$ . Consequently, the dispersion of the SOEX state is given by

$$\omega_{SOEX}(Q) = \frac{1}{2} (1 - \Delta \cos Q). \quad (5.33)$$

The SOEX state for  $x = 1/4$  is degenerate with the orbital wave excitation, see Eq. (5.3) and Fig. 14(a). When  $\Delta = 1$  and  $x = y > 0.25$ , there is a quasi-SOEX state inside the spin-orbital continuum for  $Q < \pi$ , with  $\xi < 1$ . When  $x \neq y$ , the residual signal of the SOEX state denoted by finite  $\xi$  vanishes and the BS  $\omega_{BS,2}(\pi)$  appears. The smaller the  $\Delta$  is, the more values of  $Q$  give  $\omega_{BS,2}(Q)$ . There is no BS at  $Q = \pi$  for  $y - \Delta x > (3\Delta + 1)/4$ . Furthermore, away from the symmetric point, the SOEX will acquire a finite linewidth due to residual interactions into magnon-orbion pairs,

$$\Gamma = \Im\{G^{-1}(Q, \omega)\}. \quad (5.34)$$

The exciton spectral weight can be calculated from the self-energy  $\Sigma(Q, \omega)$ ,

$$z_Q = \left[ 1 - \left( \frac{\partial \Sigma(Q, \omega)}{\partial \omega} \right) \right]^{-1} \Big|_{\omega_{\text{SOEX}}(Q)}, \quad (5.35)$$

where the SOEX energy is given by the pole,

$$\omega_{\text{SOEX}}(Q) = \Re\{G^{-1}(Q, \omega)\}. \quad (5.36)$$

If  $\Gamma/[\omega - \omega_{\text{SOEX}}(Q)]^2 \rightarrow 0$ , the exciton is stable. The decay rate of the SOEX increases with growing  $x > 1/4$  and also for decreasing momenta  $Q$ , and they coincide at  $\Delta = 0$ .

In the limit of Ising orbital interactions ( $\Delta = 0$ ), the orbital part becomes classical and orbitons are dispersionless, indicating localized orbital excitations, see Fig. 16. We find that two BSs,  $\omega_{\text{BS},1}(0)$  and  $\omega_{\text{BS},2}(0)$ , exist when  $y < 1/4$ , and there are no BSs otherwise. In contrast, at  $Q = \pi$  one finds two solutions,  $\omega_{\text{BS},1}(\pi)$  and  $\omega_{\text{BS},2}(\pi)$ , when  $-1/4 < y < 1/4$  and no BS is found for  $y > 1/4$ . In Fig. 16, both BSs,  $\omega_{\text{BS},1}$  and  $\omega_{\text{BS},2}$ , are undamped. In this case,  $\omega_T(Q) = 1/4 + x$  and is degenerate with the lower boundary of the continuum  $\omega_c(Q) = 1/4 + x$ . Moreover,  $\omega_{\text{SOEX}}(Q) = x + y$ , and especially when  $x = y = 1/4$ , these excitations coincide. In this case all excitations are dispersionless, see Fig. 16. The spin-orbital BS in Fig. 16 appears below the bottom of the spin-orbital continuum and is stabilized by its binding energy.

## VI. VON NEUMANN ENTROPY SPECTRA

### A. The spectra in the FM/FO phase

To investigate the degree of entanglement of spin-orbital excited states, we introduce the vNE spectral function in the Lehmann representation,

$$\mathcal{S}_{\text{vN}}(Q, \omega) = - \sum_n \text{Tr}\{\rho_S^{(\mu)} \log_2 \rho_S^{(\mu)}\} \delta\{\omega - \omega_n(Q)\}, \quad (6.1)$$

where we use a short-hand notation  $(\mu) = (Q, \omega_n)$  for momentum  $Q$  and excitation energy  $\omega$ , and

$$\rho_S^{(n)} = \text{Tr}_T |\Psi_n(Q)\rangle \langle \Psi_n(Q)| \quad (6.2)$$

is the spin ( $S$ ) density matrix obtained by tracing over the orbital ( $T$ ) degrees of freedom. In Fig. 17 we present the analytic results for the vNE spectral function when  $\Delta = 0.5$ ,  $x = 0.375$ , and  $y = 0.125$ . The parity symmetry is broken at  $x \neq y$  and  $\Delta \neq 1$ . The even and odd excitations show diverse behavior of their entanglement, as is displayed in Fig. 17. Inspection of the vNE spectra shows that the entanglement reaches a local maximum at the BSs and SOEX states, and all these states have short-range correlation length  $\xi$ .

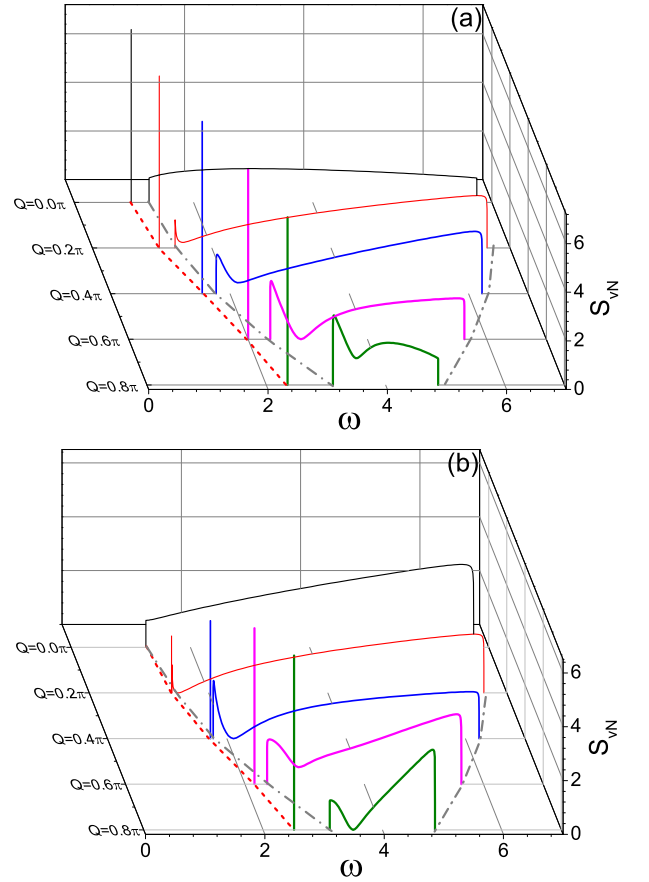


FIG. 17. (Color online) The vNE spectral function  $\mathcal{S}_{\text{vN}}(Q, \omega)$  (6.1) for the anisotropic spin-orbital  $\text{SU}(2) \otimes \text{XXZ}$  model (2.1) with  $\Delta = 0.5$  on a ring of  $L = 160$  sites, see Fig. 14(b), obtained for different momenta  $Q \leq 0.8\pi$ , and for: (a) even excitations, and (b) odd excitations. Isolated vertical lines below the continuum indicate the BS, with dispersion given by the dashed (red) line. Parameters:  $x = 0.375$ ,  $y = 0.125$ .

We have derived an asymptotic form of the vNE as a function of  $\xi$  [43],

$$\mathcal{S}_{\text{vN}} \simeq \log_2 \left\{ \frac{L}{(1 + \xi)} \right\}. \quad (6.3)$$

One finds the asymptotic logarithmic scaling of vNE of spin-orbital BSs and SOEX state whose magnon-orbitons correlation length is short-range, and the vNE is given by

$$\mathcal{S}_{\text{vN}} = \log_2 L + c_0. \quad (6.4)$$

In particular,  $c_0 = 0$  for the SOEX state and  $c_0 < 0$  otherwise. Such relation is displayed in Fig. 18. Fig. 15 implies that  $\omega_{\text{BS},1}$  are always stable for all momenta while  $\omega_{\text{BS},2}$  are undamped for large momenta.

When both  $x$  and  $y$  are away from  $1/4$ , the SOEX state is unstable and decays into a spinon and an orbiton. In this case the correlation length  $\xi$  becomes extensive. We have verified that the scaling is entirely different in such

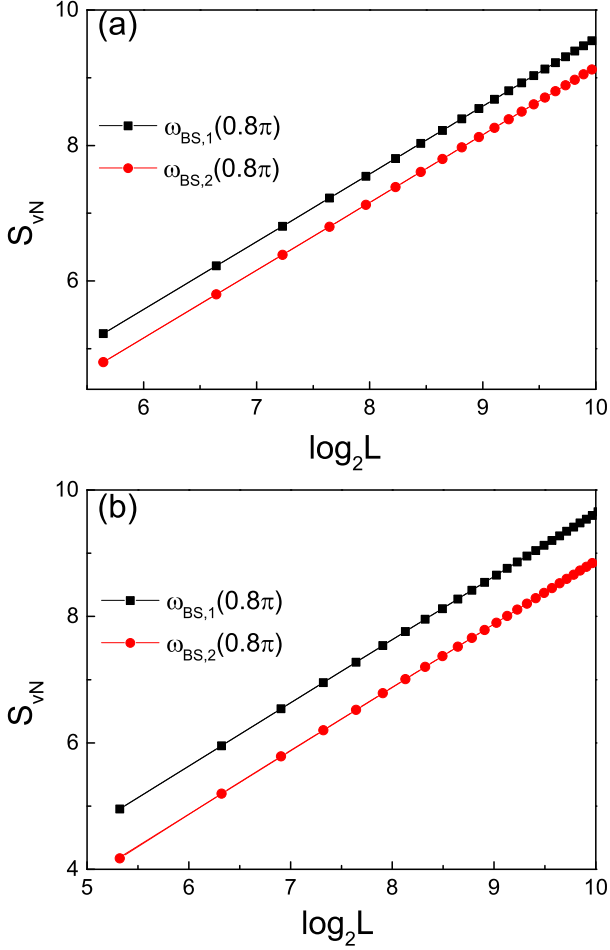


FIG. 18. (Color online) Scaling behavior of the entanglement entropy  $S_{vN}$  of the spin-orbital BSs at  $Q = 0.8\pi$  (points) for  $x = 0.375$ ,  $y = 0.125$ , and for: (a)  $\Delta = 0.5$  and (b)  $\Delta = 0$ . Lines represent logarithmic fits to Eq. (6.4) with: (a)  $c_0 = -0.421$  and  $-0.842$ ; (b)  $c_0 = -0.368$  and  $-1.122$ .

a case and the entropy of the SOEX scales instead as a power law,

$$S_{vN} = \frac{c_1}{L} + c_0. \quad (6.5)$$

The vNE saturates in the thermodynamic limit.

### B. RIXS spectral functions in the FM/FO state

The entanglement spectral function  $S_{vN}(Q, \omega)$  has a similar form as any other dynamical spin or charge correlation function. There is, however, an important difference — as there is no direct probe for the vNE of an arbitrary state, the SOE spectra can be calculated but cannot be measured directly. On the other hand, we have shown before [43] that the intensity distribution of certain RIXS spectra of spin-orbital excitations in fact probe qualitatively SOE.

We introduce the spectral function of the coupled spin-orbital excitations at distance  $l$ ,

$$A_l(Q, \omega) = \frac{1}{\pi} \lim_{\eta \rightarrow 0} \text{Im} \langle 0 | \Gamma_Q^{(l)\dagger} \frac{1}{\omega + E_0 - H - i\eta} \Gamma_Q^{(l)} | 0 \rangle. \quad (6.6)$$

Here

$$\Gamma_Q^{(0)} = \frac{1}{\sqrt{L}} \sum_j e^{iQj} S_j^- T_j^- \quad (6.7)$$

is the local operator for an on-site joint spin-orbital excitation measured in RIXS [57–59]. We employ as well the even and odd parity operators,

$$\Gamma_Q^{(1\pm)} = \frac{1}{\sqrt{2L}} \sum_j e^{iQj} (S_{j+1}^- \pm S_{j-1}^-) T_j^-, \quad (6.8)$$

which serve to probe the nearest neighbor spin-orbital excitations.

Intuitively, the on-site spectral function  $A_0(Q, \omega)$  highlights the SOEX state. It is found that both  $\omega_{\text{SOEX}}(Q)$  and  $\omega_{\text{BS}}(Q)$  are solutions of Eq. (5.21) when  $x = y = 1/4$ . However, the weight of the BS is here zero. Now the spectral function is given by

$$A_0(Q, \omega) = \delta \{ \omega - \omega_{\text{SOEX}}(Q) \}, \quad (6.9)$$

which is confirmed in Fig. 19(a). As the point  $(x, y)$  moves away from the symmetric point, i.e.,  $x = y = 1/4$ , the BSs gain spectral weight which decreases with momentum  $Q$ . The spectral weight vanishes at  $Q = \pi$  accompanying a square-root singularity at the lower bound of the continuum, see Fig. 19(b). The  $\delta$  peak turns into

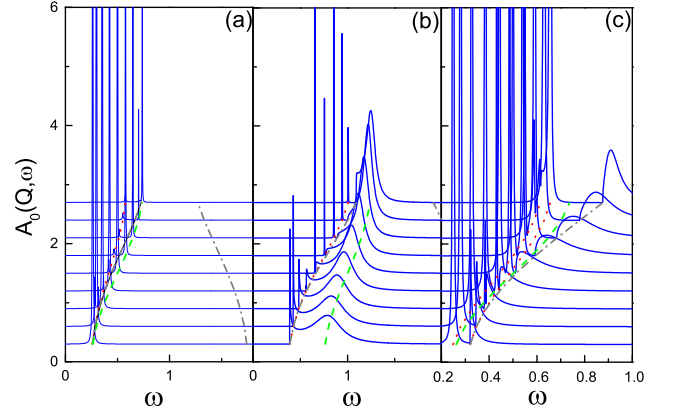


FIG. 19. (Color online) The spectral function of the on-site spin-orbital excitation  $A_0(Q, \omega)$  for the anisotropic  $\text{SU}(2) \otimes \text{XXZ}$  model with  $\Delta = 0.5$ , and for: (a)  $x = 0.25$ ,  $y = 0.25$ , (b)  $x = 0.5$ ,  $y = 0.5$ , and (c)  $x = 0.375$ ,  $y = 0.125$ . In each panel the momenta  $Q$  range from  $\pi/10$  (bottom) to  $9\pi/10$  (top); the peak broadening is  $\eta = 0.001$ . The red dotted (green dashed) lines mark the positions of BSs (SOEX) states. Gray dash-dot line signals the onset of the continuum.



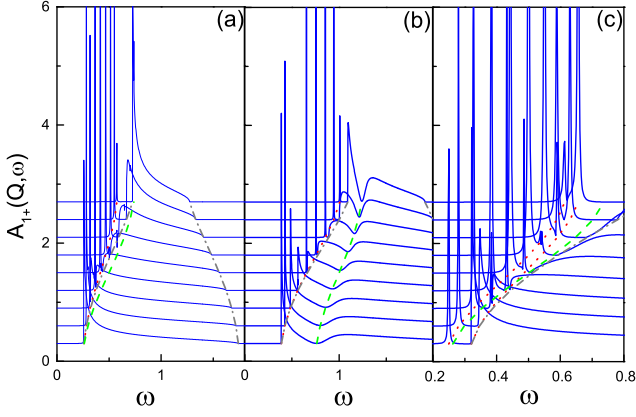


FIG. 20. (Color online) The spectral function of the spin-orbital excitation at nearest neighbors  $A_{1+}(Q, \omega)$  with even parity for the anisotropic  $SU(2) \otimes XXZ$  model with  $\Delta = 0.5$ , and for: (a)  $x = 0.25$ ,  $y = 0.25$ , (b)  $x = 0.5$ ,  $y = 0.5$ , and (c)  $x = 0.375$ ,  $y = 0.125$ . In each panel the momenta  $Q$  range from  $\pi/10$  (bottom) to  $9\pi/10$  (top); the peak broadening is  $\eta = 0.001$ . The red dotted (green dashed) lines mark the positions of BSs (SOEX) states. Gray dash-dot line signals the onset of the continuum.

a broad peak. A difference between  $x$  and  $y$  induces a second branch of BSs and it gains larger spectral weight at large momenta than the first BS, see Fig. 19(c). Altogether, the evolution of spectral weight is similar to that of the correlation length in Fig. 15.

The BSs can be captured also by the spectral func-

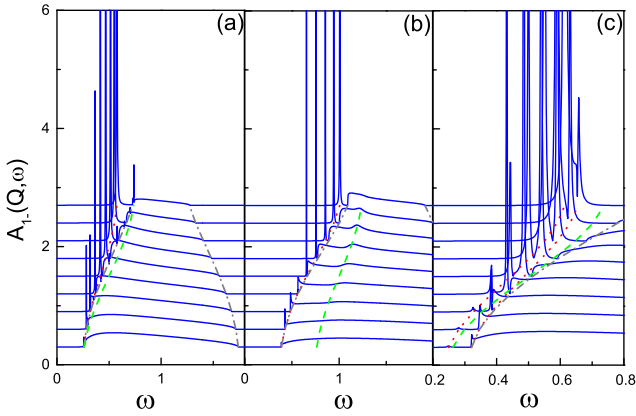


FIG. 21. (Color online) The spectral function of the spin-orbital excitation at nearest neighbors  $A_{1-}(Q, \omega)$  with odd parity for the anisotropic  $SU(2) \otimes XXZ$  model with  $\Delta = 0.5$ , and for: (a)  $x = 0.25$ ,  $y = 0.25$ , (b)  $x = 0.5$ ,  $y = 0.5$ , and (c)  $x = 0.375$ ,  $y = 0.125$ . In each panel the momenta  $Q$  range from  $\pi/10$  (bottom) to  $9\pi/10$  (top); the peak broadening is  $\eta = 0.001$ . The red dotted (green dashed) lines mark the positions of BSs (SOEX) states. Gray dash-dot line signals the onset of the continuum.

tions for the nearest neighbor excitations, see Figs. 20 and 21. With increasing momentum  $Q$ , the spectral weight of even-parity excitation  $A_{1+}(Q, \omega)$  at the first BS decreases (see Fig. 20), while the spectral weight of odd-parity excitation  $A_{1-}(Q, \omega)$  rises (see Fig. 21).  $A_{1+}(Q, \omega)$  reaches its valley for quasi-SOEX states, but no such feature could be found in  $A_{1-}(Q, \omega)$ .

## VII. DISCUSSION AND CONCLUSIONS

Motivated by the discovery of new Majumdar-Ghosh-like valence-bond spin singlet phases triggered by orbital correlations, we have studied the spin-orbital entanglement (SOE) in the one-dimensional (1D) anisotropic  $SU(2) \otimes XXZ$  spin-orbital model with the negative exchange interaction. The asymmetry between spin and orbital degrees of freedom yields a better insight into the phase diagram and the mechanisms responsible for the different types of order observed for this system. In addition to the four uniform phases I-IV, our study demonstrates that a gapful phase V exists in case of classical Ising orbital interactions, i.e., in the  $SU(2) \otimes \mathbb{Z}_2$  model. It is characterized by quadrupling of the unit cell seen as a maximum of the orbital structure factor at  $k = \pi/2$ . For  $y = -1/4$  this provides a perfect dimer structure of spin singlets in the whole region of stability of this phase, where the dimer spin correlations  $D(r)$  develop and uncover long-range dimer order. The dimer phase V is quite robust and survives when the orbital quantum fluctuations at  $\Delta > 0$  are taken into account.

The phase diagram is still richer at finite  $\Delta > 0$ , when quantum orbital fluctuations develop and induce an orbital dimer phase VI, with a complementary role of spin and orbital correlations to phase V. The emergence of the nonuniform phase V is a result of the joint interaction between spin fluctuation and orbital degree of freedom, and thus phase V carries finite SOE. The orbital fluctuations enhance the SOE in ground state near the III/V phase transition and lead to phase VI when the  $\{x, y\}$  parameters are interchanged. We also anticipate that these dimer phases may survive in higher dimensions. In fact, Lieb-Schultz-Mattis theorem is applicable to the present model for arbitrary  $x$  and  $y$  and nonzero  $\Delta$ , where a finite gap exists above these degenerate ground states. Both phases V and VI are gapped phases with alternating spin and orbital singlets, respectively. As we have shown, the phase boundaries can be captured by SOE and fidelity susceptibility. The phase transition between phases III and V is a first-order transition in the  $\Delta = 0$  case, and the transition changes to continuous when  $\Delta > 0$ .

An important consequence of finite SOE in the ground state is that it invalidates mean-field decoupling of spin and orbital degrees of freedom, as this would imply a spin-orbital product ground state. A similar restriction applies to the entangled elementary excitations in the disentangled ferromagnetic phase with ferro-orbital or-

der in spin-orbital systems which were analyzed here with the help of the von Neumann entropy spectral function. Spin-orbital excitations are highlighted by nontrivial SOE, especially by logarithmic scaling of SOE in the phase.

*A priori*, the SOE makes it necessary to treat the eigenstates of a given model exactly. In fact, since a mean-field decoupling shields the SOE, it fails to describe elementary excitations even qualitatively correctly in a number of spin-orbital models. In antiferromagnetic ground states with ferro-orbital order it was demonstrated both in theory [37] and experiment [38] that the spin-orbit excitation fractionalizes into freely propagating spin and orbiton, giving rise to spin-orbital separation under specific condition. The SOE in the spin-orbital separation remains unclear. The low-lying excitations in phases II (AF/FO) and III (AF/AO) are spin waves with vanishing SOE, corresponding to a two-spinon continuum of an antiferromagnetic spin chain. The low-lying excitation in phases V and VI corresponds to spin-orbital excitations as shown in Figs. 2(b) and 2(c). The problem of the SOE in elementary excitations in other phases remains a challenge for future studies.

Summarizing, we have shown that the anisotropic  $SU(2) \otimes XXZ$  spin-orbital model with *negative* exchange coupling has remarkably different behavior and phase diagrams from the well known  $SU(2) \otimes SU(2)$  model with *positive* exchange coupling. While the spin-orbital liquid phase is absent in the former case, we have four phases that the joint ferromagnetic/ferro-orbital fluctuations are surprisingly strong at the quantum phase transition to the antiferromagnetic spin order which gives even stronger SOE than that established for the 1D isotropic  $SU(2) \otimes SU(2)$  model with positive exchange coupling.

## ACKNOWLEDGMENTS

We thank Krzysztof Wohlfeld for insightful discussions. W.-L.Y. acknowledges support by the Natural Science Foundation of Jiangsu Province of China under Grant No. BK20141190 and the NSFC under Grant No. 11474211. A.M.O. kindly acknowledges support by Narodowe Centrum Nauki (NCN, National Science Center) under Project No. 2012/04/A/ST3/00331.

## Appendix: Phase diagrams for the two-site model

To understand better the phase boundaries in the anisotropic  $SU(2) \otimes XXZ$  spin-orbital model with negative exchange coupling (2.1), we present here an exact solution for the system of  $L = 2$  sites [91],

$$\mathcal{H}_{12} = -J \left( \vec{S}_1 \cdot \vec{S}_2 + x \right) \times \left[ \frac{\Delta}{2} (T_1^+ T_2^- + T_1^- T_2^+) + T_1^z T_2^z + y \right], \quad (\text{A.1})$$

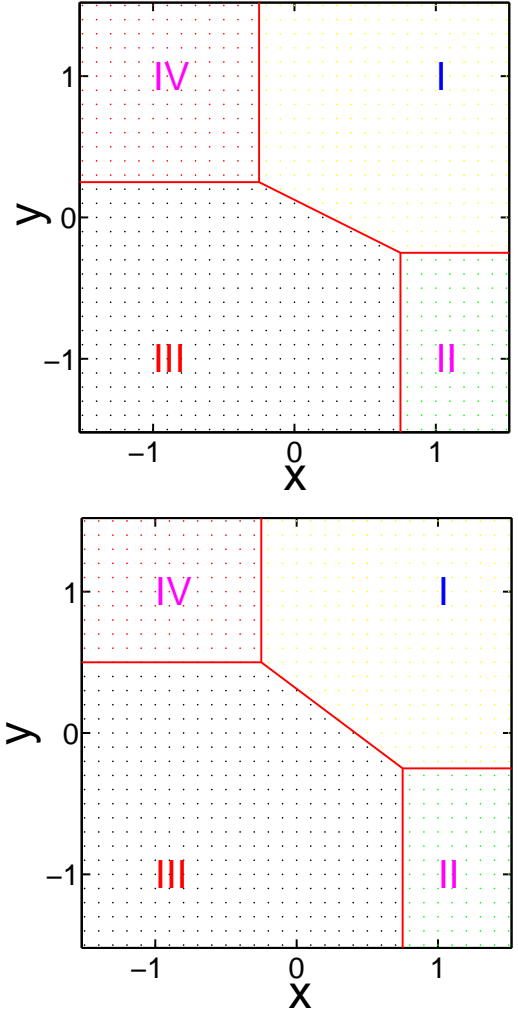


FIG. 22. (Color online) (a) The phase diagram of 2-site model when  $\Delta = 0$ . (b)  $\Delta = 0.5$ . Phases I-IV correspond to FS/FO, AS/FO, AS/AO, FS/AO configurations in spin-orbital sectors.

Again,  $\{x, y\}$  are the parameters, and  $0 \leq \Delta \leq 1$  interpolates between the Ising  $\mathbb{Z}_2$  ( $\Delta = 0$ ) and Heisenberg  $SU(2)$  ( $\Delta = 1$ ) symmetry. The orbital interaction with  $XXZ$  symmetry can be exactly diagonalized and one finds 4 eigenstates:  $|++\rangle$ ,  $|--\rangle$ ,  $(|+-\rangle + |-+\rangle)/\sqrt{2}$ ,  $(|+-\rangle - |-+\rangle)/\sqrt{2}$ , corresponding to eigenvalues:  $1/4$ ,  $1/4$ ,  $\Delta/2 - 1/4$ ,  $-\Delta/2 - 1/4$ , respectively. At  $\Delta = 0$  we recover doubly degenerate configurations from the latter two, while at  $\Delta = 1$  we recover a triplet  $T = 1$  from the first three. In any case, the third component of the triplet,  $(|+-\rangle + |-+\rangle)/\sqrt{2}$ , is always an entangled excited state with the present choice of parameters, while the orbital singlet,  $(|+-\rangle - |-+\rangle)/\sqrt{2}$ , is an entangled ground state for some parameters.

The spin part is classified as a triplet  $S = 1$  or a singlet  $S = 0$ , and these states are accompanied by the orbital states described above. This gives the states I-IV in Table

TABLE II. The spin-orbital configuration for the model (A.1), with phases I-IV defined by distinct spin  $S$  and orbital state as as obtained at  $0 < \Delta < 1$ . The lowest energy  $E^0/J$  has degeneracy  $d$  and becomes the ground state at the respective values of  $\{x, y\}$  parameters, Fig. 22. At  $\Delta = 0$  the degeneracies of phases III and IV change to 2 and 6 for the  $\mathbb{Z}_2 \otimes \mathbb{Z}_2$  symmetry, while at  $\Delta = 1$  the degeneracies for the ground states I-IV are 9, 3, 1, 3 and follow from the  $SU(2) \otimes SU(2)$  symmetry.

phase	$S$	orbital states	$E^0/J$	$d$
I	1	$ ++\rangle,  --\rangle$	$-(\frac{1}{4} + x)(\frac{1}{4} + y)$	6
II	0	$ ++\rangle,  --\rangle$	$-(\frac{3}{4} + x)(\frac{1}{4} + y)$	2
III	0	$\frac{1}{\sqrt{2}}( +-\rangle -  -+\rangle)$	$(-\frac{3}{4} + x)(\frac{1}{4} + \frac{\Delta}{2} - y)$	1
IV	1	$\frac{1}{\sqrt{2}}( +-\rangle -  -+\rangle)$	$(\frac{1}{4} + x)(\frac{1}{4} + \frac{\Delta}{2} - y)$	3

II, and one of them is the ground state for any point in the  $(x, y)$  plane. All phase transitions are first order, with a change of spin or orbital state. The phases II and IV are symmetric for  $\Delta = 1$ , and the transition between I and III occurs along the  $x + y = 1/2$  line [43]. At  $\Delta = 0$  phase IV exists for  $y > 1/4$  while phase II only for  $x > 3/4$ , see Fig.

22(a). This reflects the essential difference between the orbital configurations in the Ising limit and the quantum spin states. Note that spin singlet  $S = 0$  is an entangled state, but the larger Hilbert space gives no spin-orbital entanglement in any phase. Thus, the total energies and the phase diagram are easily deduced, see Fig. 22.

From the comparison of the energies  $E^0$  of phases III and IV (Table II) one can see that the boundary between III and IV, given by the straight line  $y = 1/4 + \Delta/2$ , moves upwards with increasing  $\Delta$ , see Fig. 22(b). Accordingly, the phase boundary between phases I and III is also modified. The interplay between spins and orbitals develops and leads to interesting consequences of entanglement for rings with  $L \geq 4$ . Remarkably, the trivial phase diagram found for Ising-Ising interactions for  $L = 2$  sites (with II-III and IV-III transition lines at  $x = 1/4$  and  $y = 1/4$ , similar to the diagrams in Fig. 22) is the same for the  $\mathbb{Z}_2 \otimes \mathbb{Z}_2$  spin-orbital model in the thermodynamic limit,

$$\mathcal{H}_{\mathbb{Z}_2 \otimes \mathbb{Z}_2} = -J \sum_j (S_j^z S_{j+1}^z + x) (T_j^z T_{j+1}^z + y). \quad (\text{A.2})$$

- 
- [1] K. I. Kugel and D. I. Khomskii, JETP **37**, 725 (1973); Sov. Phys. Usp. **25**, 231 (1982).
- [2] L. F. Feiner, A. M. Oleś, and J. Zaanen, Phys. Rev. Lett. **78**, 2799 (1997); J. Phys.: Condens. Matter **10**, L555 (1998).
- [3] Y. Tokura and N. Nagaosa, Science **288**, 462 (2000).
- [4] A. M. Oleś, G. Khaliullin, P. Horsch, and L. F. Feiner, Phys. Rev. B **72**, 214431 (2005).
- [5] G. Khaliullin, Prog. Theor. Phys. Suppl. **160**, 155 (2005).
- [6] A. M. Oleś, J. Phys.: Condens. Matter **24**, 313201 (2012); Acta Phys. Polon. A **127**, 163 (2015).
- [7] Yi Li, E. H. Lieb, and C. Wu, Phys. Rev. Lett. **112**, 217201 (2014).
- [8] E. Zhao and W. V. Liu, Phys. Rev. Lett. **100**, 160403 (2008).
- [9] C. Wu, Phys. Rev. Lett. **100**, 200406 (2008); C. Wu and S. Das Sarma, Phys. Rev. B **77**, 235107 (2008).
- [10] G. Sun, G. Jackeli, L. Santos, and T. Vekua, Phys. Rev. B **86**, 155159 (2012).
- [11] V. Galitski and I. B. Spielman, Nature **494**, 49 (2013).
- [12] Z. Zhou, E. Zhao, and W. V. Liu, Phys. Rev. Lett. **114**, 100406 (2015).
- [13] G. Jackeli and G. Khaliullin, Phys. Rev. Lett. **102**, 017205 (2009).
- [14] M. Z. Hasan and C. L. Kane, Rev. Mod. Phys. **82**, 3045 (2010).
- [15] B. J. Kim, H. Jin, S. J. Moon, J.-Y. Kim, B.-G. Park, C. S. Leem, J. Yu, T. W. Noh, C. Kim, S.-J. Oh, J.-H. Park, V. Durairaj, G. Cao, and E. Rotenberg, Phys. Rev. Lett. **101**, 076402 (2008).
- [16] R. Comin, G. Levy, B. Ludbrook, Z.-H. Zhu, C. N. Veenstra, J. A. Rosen, Y. Singh, P. Gegenwart, D. Stricker, J. N. Hancock, D. van der Marel, I. S. Elfimov, and A. Damascelli, Phys. Rev. Lett. **109**, 266406 (2012); F. Trouselet, M. Berciu, A. M. Oleś, and P. Horsch, *ibid.* **111**, 037205 (2013).
- [17] G. Khaliullin, Phys. Rev. Lett. **111**, 197201 (2013).
- [18] A. Akbari and G. Khaliullin, Phys. Rev. B **90**, 035137 (2014).
- [19] A. M. Oleś, P. Horsch, L. F. Feiner, and G. Khaliullin, Phys. Rev. Lett. **96**, 147205 (2006).
- [20] W. Brzezicki, J. Dziarmaga, and A. M. Oleś, Phys. Rev. Lett. **112**, 117204 (2014).
- [21] M. Y. Kagan, K. I. Kugel, A. V. Mikheyenkov, and A. F. Barabanov, JETP Lett. **100**, 187 (2014).
- [22] W. Brzezicki, A. M. Oleś, and M. Cuoco, Phys. Rev. X **5**, 011037 (2015).
- [23] S. Mühlbauer, B. Binz, F. Jonietz, C. Pfleiderer, A. Rosch, A. Neubauer, R. Georgii, and P. Böni, Science **323**, 915 (2009).
- [24] C. Z. Chang, J. Zhang, X. Feng, J. Shen, Z. Zhang, M. Guo, K. Li, Y. Ou, P. Wei, L. L. Wang, Z. Q. Ji, Y. Feng, S. Ji, X. Chen, J. Jia, X. Dai, Z. Fang, S. C. Zhang, K. He, Y. Wang, L. Lu, X. C. Ma, and Q. K. Xue, Science **340**, 167 (2013).
- [25] X. Wan, A. M. Turner, A. Vishwanath, and S. Y. Savrasov, Phys. Rev. B **83**, 205101 (2011).
- [26] Z.-H. Zhu, C. N. Veenstra, G. Levy, A. Ubaldini, P. Syers, N. P. Butch, J. Paglione, M. W. Haverkort, I. S. Elfimov, and A. Damascelli, Phys. Rev. Lett. **110**, 216401 (2013).
- [27] Z.-H. Zhu, A. Nicolaou, G. Levy, N. P. Butch, P. Syers, X. F. Wang, J. Paglione, G. A. Sawatzky, I. S. Elfimov, and A. Damascelli, Phys. Rev. Lett. **111**, 216402 (2013).
- [28] Y. Ishiguro, K. Kimura, S. Nakatsuji, S. Tsutsui, A. Q. R. Baron, T. Kimura, and Y. Wakabayashi, Nat. Commun. **4**, 3022 (2013).
- [29] N. Katayama, K. Kimura, Y. Han, J. Nasu, N. Drichko, Y. Nakanishi, M. Halim, Y. Ishiguro, R. Satake, E. Nishibori, M. Yoshizawa, T. Nakano, Y. Nozue, Y. Wakabayashi, S. Ishihara, M. Hagiwara, H. Sawa, S. Nakat-

- suji, Proc. Nat. Ac. Sci. **112**, in press (2015).
- [30] Leon Balents, Nature **464**, 199 (2010).
- [31] L. Mittelstädt, M. Schmidt, Z. Wang, F. Mayr, V. Tsurkan, P. Lunkenheimer, D. Ish, L. Balents, J. Deisenhofer, and A. Loidl, Phys. Rev. B **91**, 125112 (2015).
- [32] N. J. Laurita, J. Deisenhofer, L. D. Pan, C. M. Morris, M. Schmidt, M. Johnsson, V. Tsurkan, A. Loidl, and N. P. Armitage, Phys. Rev. Lett. **114**, 207201 (2015).
- [33] B. Normand and A. M. Oleś, Phys. Rev. B **78**, 094427 (2008); B. Normand, *ibid.* **83**, 064413 (2011); J. Chaloupka and A. M. Oleś, *ibid.* **83**, 094406 (2011).
- [34] P. Corboz, M. Lajkó, A. M. Läuchli, K. Penc, and F. Mila, Phys. Rev. X **2**, 041013 (2012).
- [35] A. Smerald and F. Mila, Phys. Rev. B **90**, 094422 (2014).
- [36] L. J. P. Ament, M. van Veenendaal, T. P. Devereaux, J. P. Hill, and J. van den Brink, Rev. Mod. Phys. **83**, 705 (2011).
- [37] K. Wohlfeld, M. Daghofer, S. Nishimoto, G. Khaliullin, and J. van den Brink, Phys. Rev. Lett. **107**, 147201 (2011); K. Wohlfeld, S. Nishimoto, M. W. Haverkort, and J. van den Brink, Phys. Rev. B **88**, 195138 (2013).
- [38] J. Schlappa, K. Wohlfeld, K. J. Zhou, M. Mourigal, M. W. Haverkort, V. N. Strocov, L. Hozoi, C. Monney, S. Nishimoto, S. Singh, A. Revcolevschi, J.-S. Caux, L. Patthey, H. M. Rønnow, J. van den Brink, and T. Schmitt, Nature **485**, 82 (2012).
- [39] J. Kim, D. Casa, M. H. Upton, T. Gog, Y.-J. Kim, J. F. Mitchell, M. van Veenendaal, M. Daghofer, J. van den Brink, G. Khaliullin, and B. J. Kim, Phys. Rev. Lett. **108**, 177003 (2012).
- [40] Z. Wang, M. Schmidt, A. Günther, S. Schaile, N. Pascher, F. Mayr, Y. Goncharov, D. L. Quintero-Castro, A. T. M. N. Islam, B. Lake, H.-A. Krug von Nidda, A. Loidl, and J. Deisenhofer, Phys. Rev. B **83**, 201102(R) (2011).
- [41] J. B. Goodenough, *Magnetism and the Chemical Bond* (Wiley Interscience, New York, 1963).
- [42] L. Amico, R. Fazio, A. Osterloh, and V. Vedral, Rev. Mod. Phys. **80**, 517 (2008).
- [43] W.-L. You, A. M. Oleś, and P. Horsch, Phys. Rev. B **86**, 094412 (2012).
- [44] J. Eisert, M. Cramer, and M. B. Plenio, Rev. Mod. Phys. **82**, 277 (2010).
- [45] Lluís Masanes, Phys. Rev. A **80**, 052104 (2009).
- [46] I. Hagymási, J. Sólyom, and Ö. Legeza, Phys. Rev. B **92**, 035108 (2015).
- [47] Y. Chen, Z. D. Wang, Y. Q. Li, and F. C. Zhang, Phys. Rev. B **75**, 195113 (2007).
- [48] R. Lundgren, V. Chua, and G. A. Fiete, Phys. Rev. B **86**, 224422 (2012).
- [49] R. Berkovits, Phys. Rev. Lett. **108**, 176803 (2012); Phys. Rev. B **87**, 075141 (2013).
- [50] W.-L. You, A. M. Oleś, and P. Horsch, New J. Phys. **17**, in press (2015).
- [51] D. Gottesman and M. B. Hastings, New J. Phys. **12**, 025002 (2010).
- [52] P. Calabrese and J. Cardy, J. Stat. Mech. P06002 (2004).
- [53] R. Helling, H. Leschke, and W. Spitzer, Int. Math. Res. Not. **2011**, 1451 (2011).
- [54] L.-A. Wu, M. S. Sarandy, and D. A. Lidar, Phys. Rev. Lett. **93**, 250404 (2004).
- [55] V. Alba, M. Fagotti, and P. Calabrese, J. Stat. Mech. P10020 (2009).
- [56] Y.-Q. Li, M. Ma, D.-N. Shi, and F.-C. Zhang, Phys. Rev. Lett. **81**, 3527 (1998); B. Frischmuth, F. Mila, and M. Troyer, *ibid.* **82**, 835 (1999).
- [57] L. J. P. Ament, G. Ghiringhelli, M. M. Sala, L. Braicovich, and J. van den Brink, Phys. Rev. Lett. **103**, 117003 (2009).
- [58] V. Bisogni, K. Wohlfeld, S. Nishimoto, C. Monney, J. Trinckauf, K. Zhou, R. Kraus, K. Koepf, C. Sekar, V. Strocov, B. Büchner, T. Schmitt, J. van den Brink, and J. Geck, Phys. Rev. Lett. **114**, 096402 (2015).
- [59] Cheng-Chien Chen, M. van Veenendaal, T. P. Devereaux, and K. Wohlfeld, Phys. Rev. B **91**, 165102 (2015).
- [60] B. Sutherland, Phys. Rev. B **12**, 3795 (1975).
- [61] C. Itoi, S. Qin, and I. Affleck, Phys. Rev. B **61**, 6747 (2000); E. Orignac, R. Citro, and N. Andrei, Phys. Rev. B **61**, 11533 (2000).
- [62] Y. Yamashita, N. Shibata, and K. Ueda, J. Phys. Soc. Jpn. **69**, 242 (2000).
- [63] Peng Li and Shun-Qing Shen, Phys. Rev. B **72**, 214439 (2005).
- [64] A. K. Kolezhuk and H.-J. Mikeska, Phys. Rev. Lett. **80**, 2709 (1998).
- [65] A. K. Kolezhuk, H.-J. Mikeska, and U. Schollwöck, Phys. Rev. B **63**, 064418 (2001).
- [66] M. J. Martins and B. Nienhuis, Phys. Rev. Lett. **85**, 4956 (2000).
- [67] F. Mila, B. Frischmuth, A. Deppeler, and M. Troyer, Phys. Rev. Lett. **82**, 3697 (1999).
- [68] G. Khaliullin, P. Horsch, and A. M. Oleś, Phys. Rev. Lett. **86**, 3879 (2001); Phys. Rev. B **70**, 195103 (2004).
- [69] K. I. Kugel, D. I. Khomskii, A. O. Sboychakov, and S. V. Streltsov, Phys. Rev. B **91**, 155125 (2015).
- [70] W.-L. You, Y.-W. Li, and S.-J. Gu, Phys. Rev. E **76**, 022101 (2007).
- [71] M. Daghofer, K. Wohlfeld, A. M. Oleś, E. Arrigoni, and P. Horsch, Phys. Rev. Lett. **100**, 066403 (2008); K. Wohlfeld, M. Daghofer, A. M. Oleś, and P. Horsch, Phys. Rev. B **78**, 214423 (2008).
- [72] G.-W. Chern and N. Perkins, Phys. Rev. B **80**, 220405(R) (2009); G.-W. Chern, N. Perkins, and G. I. Japaridze, *ibid.* **82**, 172408 (2010).
- [73] B. Douçot, M. V. Feigel'man, L. B. Ioffe, and A. S. Ioselevich, Phys. Rev. B **71**, 024505 (2005); Z. Nussinov and E. Fradkin, *ibid.* **71**, 195120 (2005).
- [74] W. Brzezicki and A. M. Oleś, Phys. Rev. B **82**, 060401 (2010); *ibid.* **87**, 214421 (2013); *ibid.* **90**, 024433 (2014); L. Cincio, J. Dziarmaga, and A. M. Oleś, *ibid.* **82**, 104416 (2010).
- [75] F. Trouselet, A. M. Oleś, and P. Horsch, Europhys. Lett. **91**, 40005 (2010); Phys. Rev. B **86**, 134412 (2012).
- [76] A. Kitaev, Ann. Phys. (NY) **321**, 2 (2006).
- [77] Z. Nussinov and J. van den Brink, Rev. Mod. Phys. **87**, 1 (2015).
- [78] T.-H. Han, J. S. Helton, S. Chu, D. G. Nocera, J. A. Rodriguez-Rivera, C. Broholm, and Y. S. Lee, Nature **492**, 406 (2012).
- [79] C. K. Majumdar and D. Ghosh, J. Math. Phys. **10**, 1388 (1969).
- [80] Y. Yu, G. Müller, and V. S. Viswanath, Phys. Rev. B **54**, 9242 (1996).
- [81] A. A. Nersisyan and A. M. Tsvelik, Phys. Rev. Lett. **78**, 3939 (1997); A. Nersisyan, G.-W. Chern, and N. B. Perkins, Phys. Rev. B **83**, 205132 (2011).
- [82] Z. G. Soos, S. Kuwajima, and J. E. Mihalick, Phys. Rev.



- B **32**, 3124 (1985).
- [83] G. Spronken, B. Fourcade, and Y. Lépine, Phys. Rev. B **33**, 1886 (1986).
  - [84] S.-J. Gu, G.-S. Tian, and H.-Q. Lin, Chin. Phys. Lett. **24**, 2737 (2007).
  - [85] W. Brzezicki, J. Dziarmaga, and A. M. Oleś, Phys. Rev. Lett. **109**, 237201 (2012); Phys. Rev. B **87**, 064407 (2013); Acta Phys. Pol. A **126**, A-40 (2014).
  - [86] J. Sirker, A. Herzog, A. M. Oleś, and P. Horsch, Phys. Rev. Lett. **101**, 157204 (2008).
  - [87] W. Brzezicki and A. M. Oleś, Phys. Rev. B **90**, 024433 (2014).
  - [88] A. Herzog, P. Horsch, A. M. Oleś, and J. Sirker, Phys. Rev. B **83**, 245130 (2011).
  - [89] M. Wortis, Phys. Rev. **132**, 85 (1963).
  - [90] T. Schneider, Phys. Rev. B **24**, 5327 (1981).
  - [91] J. van den Brink, W. Stekelenburg, D. I. Khomskii, G. A. Sawatzky, and K. I. Kugel, Phys. Rev. B **58**, 10276 (1998).
  - [92] J. Bała, A. M. Oleś, and G. A. Sawatzky, Phys. Rev. B **63**, 134410 (2001).
  - [93] S. Cojocaru and A. Ceulemans, Phys. Rev. B **67**, 224413 (2003).

